UNIVERSITY OF THE PELOPONNESE
DEPARTMENT OF HISTORY, ARCHAEOLOGY
AND CULTURAL RESOURCES MANAGEMENT

NATIONAL CENTER
FOR SCIENTIFIC RESEARCH
"DEMOKRITOS"

NATIONAL
OBSERVATORY
OF ATHENS

Master of Science in
«Cultural Heritage Materials and Technologies»

PAIGE VAN TASSEL
(R.N. 1012201802004)

DIPLOMA THESIS:

CORROSION STUDY OF GLASS MOSAIC TESSERAE AT THE ARCHAEOLOGICAL SITE OF STOBI, NORTH MACEDONIA

SUPERVISING COMMITTEE:
- Prof. Nikolaos Zacharias
- Assoc. Prof Eleni Palamara

EXAMINATION COMMITTEE:
- Dr. Nikolaos Zacharias
- Prof. Eleni Palamara
- Dr. Andreas Karydas

ΚΑΛΑΜΑΤΑ, OCTOBER 2020

Abstract

The present MSc thesis focuses on the historical and material analytical investigation of 4th century CE glass tesserae found at the archaeological site of Stobi, North Macedonia. The purpose of this study is to aid in further understanding the manufacturing process used to create the glass tesserae found between the 1st and 4th century CE at the archaeological site of Stobi. This will require a historical investigation into the contextual evidence of glass use found at the archaeological site throughout the region of Macedonia Secunda during the 1st to 4th century CE. The analytical investigation involves the use of portable X-ray Fluorescence, Scanning Electron Microscopy – Electron Dispersive Spectroscopy, and Reflected Light Microscopy to characterize and identify the raw materials used in the production of these tesserae and the degradation products of the glass tesserae. The use of these analytical techniques chosen for these glass tesserae can aid in further understanding of the historical trade that took place at the ancient city of Stobi.

Contents

List of Figures

Acknowledgements

I would like to thank the following people for assisting me with this research:

Prof. Nikos Zacharias for the supervision and guidance of this project. Dr. Eleni Palamara for training on the Scanning Electron Microscope and portable X-Ray Fluorescence. University the Peloponnese Archaeometry Lab in Kalamata, Greece for use of the Scanning Electron Microscope and portable X-Ray Fluorescence. National Institute Stobi in North Macedonia, notably Silvana Blazevska, Former Director, and Spase Perovski, Current Director, for sampling permission and access to collections. Mishko Tutkovski, Interim Director, for guidance in the conservation treatment and art historical information associated with the wall mosaic fragments. Jovan Radjanski and Goce Pavlovski for the archaeological context and history of Stobi as well as the context and history associated with the wall mosaic fragments. Bilijana Peeva and Dimitar Nikolovski for the historical information and condition of glass collections at the archaeological site of Stobi. I extend my gratitude to the Queen's University Art Conservation Program in Kingston, Ontario, Canada for access and use of the microscopy lab and sample preparation materials.

1. Introduction

This project will briefly review the technological development of glass in the Mediterranean region, then focus on Roman glassmaking, production, and sources from the 1st century CE onwards. Then, overview the current studies on the composition of glass tesserae made in the late Roman period throughout the Mediterranean area. After the brief historical outline of glass development in the Mediterranean region during the Roman period, there will be an introduction to the site of Stobi, North Macedonia, and its historical development in the early and late Roman period. This will include the use of mosaic decoration throughout the site and the specific context in which the glass tesserae analysed were found. Following the experimental set up and instrumentation used, there will be a description of the results. This thesis will be concluded by a discussion on future research work to be done on the archaeological site of Stobi.

1.1Technological development of glass in the Mediterranean region

The first evidence of man-made glass derived in the middle eastern Mesopotamian region from 2500 BCE where they were experimenting with glazing materials to create what is known as faience to imitate rare stones such as turquoise (Tait, 1991, 26). It is thought that the reign of Thutmose III, who conducted several successful campaigns in Syria, caused an influx of skilled Syrian craftsmen working in Egyptian workshops, causing an exchange of recipes and materials between Middle Eastern and Egyptian glass making techniques (Tait, 1991, 26). The first glass vessels were produced around 1500 BCE and shortly thereafter the Egyptian glass industry was born. Around 1200 BCE, the Egyptians had nearly perfected glassmaking techniques including mold casting to produce cups, bowls and dishes which was not feasible by previous core molding methods (Rasmussen, 2012, 26).

There was a period of turmoil in the Mediterranean between 1200 and 1000 BCE, during the Late Bronze age, causing a near collapse in the glass making industry (Rasmussen, 2012, 27). It was not until the 9th century BCE that these techniques travelled throughout the Mediterranean region (Tait, 1991, 38). The use of core formed vessels had their origins in the Mesopotamian region in the 5th century BCE as described above, however, developed in style and flourished during the Hellenistic period due to the influence of the shape of the Greek vases made from pottery and metal (Rasmussen, 2012, 28). The technique of core formed vessels, seen in figure 1 below, uses a metal or wooden rod to manipulate molten glass into

shape. Figure 2 shows the mold casting method; both these techniques were developed in Egypt and flourished during the Hellenistic period.

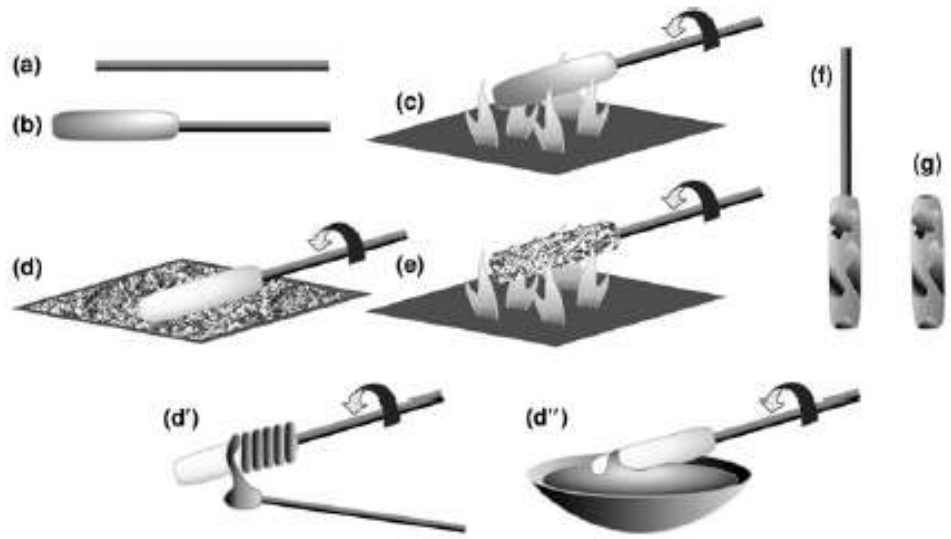

Figure 1: Core molding technique to produce core formed vessels, A: initial metal or wooden rod, B: formation of core onto the rod, C: firing to set the core, D: application of the glass via rolling in crushed glass, E: firing of applied layer, F and G: completed object with and without rod, D' alternate methods for the application of the glass including coiled strands of softened gold around the mold or D" dipping the core into molten glass. Rasmussen, pg. 25.

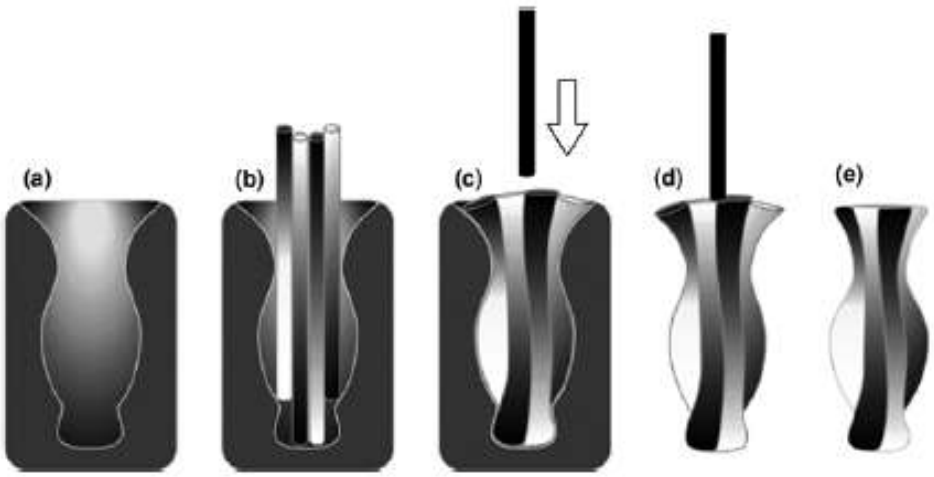

Figure 2: Fuse casting glass objects, A: glass pieces added, B: heated to fuse and fill mold, C: metal rod inserted, D: mold removed, E: piece ground and polished to finish. Rasmussen, pg. 26.

It is also during the late Hellenistic and early Roman period that we see the experimentation with glass production techniques throughout the Mediterranean such as using gold leaf, mosaic glass bowl making, slumping production techniques, among others. Slumping involved pressing a molten glass to set the design then slumping it over a stone or

metal circular object to create a bowl which can be seen in figure 3 below. This type of technique would have been created for the social elite who request specific pressed designs (Rasmussem, 2012, 31)

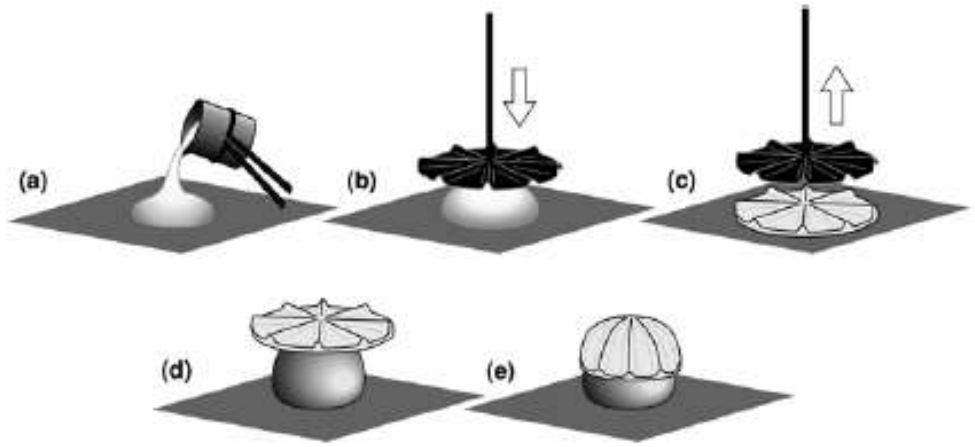

Figure 3: Slumping technique, Rasmussen, pg 32.

At around 50 CE blown glass, both free form and mold blown, were the preferred technique of glass makers in the Mediterranean region and core formed techniques fell out of favour (Tait, 1991, 57). Non-blown molded glass continued to be used for more decorative pieces such as jewellery, inlays, pendants, among other items. Blown glass allowed for thin transparent glass to be created through the method of blowing inside molten glass through a hollow iron tube and subsequent shaping with additional tools.

1.1.I. Primary and secondary production centers in the Roman period

The types of glass production that took place in each city was dependant on whether there were a primary or secondary production center. The primary production centers in the Roman period were those who had immediate access to the ingredients to create glass including silica and an alkali source, largely natron, in the Roman period. These primary production centers were necessary because of the high firing temperature needed to melt the silica and other ingredients to create glass, which could not be achieved with the smaller size of the furnace used in secondary production centers (Henderson, 2013, 216). These primary production centers would be responsible for creating bulk glass sheets, rods, and ingots to send out to the secondary production centers where the glass would be re-melted and shaped into objects for use depending on the local need such as those described in the next section of this thesis.

1.2. Glass usage in the Roman period

The development of faience and glass in ancient Egypt involved the use of the materials for personal and decorative adornment such as necklaces, amulets, and little glass figurines. The annexation of Egypt after Augustus' victory over Marc Anthony in 31 CE marked a significant moment in the history of glass usage in the Roman empire. The access to Egyptian recipes of glassmaking along with a rich source of silica had caused a larger expanse of glass usage in the Roman period (Zeitzer, 2018, 4). There were also the technical developments from core formed to blown glass in the Mediterranean region around Greece and Italy during the Roman period which allowed for a higher variety of glassware such as perfume bottles, plates, wine glasses and carafes (Rasmussen, 2012, 21). This allowed for widespread use of the material for both decorative and utilitarian purposes.

As blown glass became a popular production method, the types of glassware produced get more technically challenging and involve a play of light and colour such as the beautiful Lycurgus cage cup which was produced in the 4th century CE that has a dichroic phenomenon where the glass changes colour depending on the angle of incident light (Tait, 2012, 90). Similar types of cage cup fragments have been found at the archaeological site of Stobi, which now reside in the Archaeological Museum of Skopje.

The continual artistic innovation that took place during this time allowed for the constant fascination and consumption of glass products, whether it be for functional or decorative purposes. Glass became a social signifier of wealth in Roman period due to the increasing demand for the product in stately homes that were lavishly decorated with glassware on their shelves and cabinets, rather than simply being a utilitarian object (Zeitzer, 2018, 38). As glass became more decorative in its purpose, it showed the wealth of the patrons who used it for display rather than use. As discussed in the next section, the use of glass in wall and floor mosaics added a level of status to the patron as being able to afford the mosaics for the walls and floors but also to use glass in the construction of the piece showed the wealthy position of the person.

1.2.I. Glass tesserae in mosaics

Glass in mosaics of the floors and walls indicated the wealth of the person as well as the patronage if glass mosaics had decorated ecclesiastical buildings. Glass tesserae were used in the production of mosaic floors and walls in order to give an added shimmer to the décor that embellished the houses and basilicas of wealthy people during the late Hellenistic

and Roman period (Tait, 2012, 60). There is some evidence to suggest that some mosaics used the scraps of broken glass to create wall mosaics, however a majority of the glass used to create mosaics were cut from large glass blocks that were mass produced at primary production centers, most often located near a silica source, then shipped to local secondary centers such as Stobi (Wiseman, 1986). These glass blocks were more durable than recycled glass as it came from a primary production center, using primary source materials whereas recycled glass often changed the composition of the glass, theoretically causing a faster degradation rate (Henderson, 2013, 95)

1.3. Glass composition in the Roman period

Glass is composed of a base, flux and former heated under high temperature to create molten glass that can be shaped and formed. The base is typically silica, the flux is an alkali source that is either potash or commonly soda which was used to lower the melting point of the sand that was used. The former or stabilizer is most commonly calcium oxide, in the form of calcite or crushed shells, which was used to add stability to the glass minimizing the potential to break or dissolve in water. The alkali source was mainly natron salts originating from the Middle East, according to Pliny and his *Naturalis* books where he describes the old recipe for making glass in the Roman period. Pliny later describes the sources of silica and its role in the production of glass as well as some locations where one might find suitable glassmaking sand:

> "That part of Syria which is known as Phoenicia and borders on Judea…This is supposed to be the source of the River Belus, which after traversing a distance of 5 miles flows into the sea near the colony of Ptolemais…The beach stretches for not more than half a mile, and yet for many centuries the production of glass depended on this area alone…Sidon was once famous for its glassworks, since, apart from other achievements, glass mirrors were invented there. This was the old method of producing glass. Now, however, in Italy too, a white sand which forms in the River Volturno is found along six miles of the seashore between Cuma and Literno. Wherever it is softest, it is taken to be ground in a mortar or mill. Then it is mixed with three parts soda, either by weight or measure, and after being fused is taken in its molten state to other furnaces. There it forms a lump known in Greek as 'sand-soda'. This is again melted and forms a pure glass, and is indeed a lump of colourless glass." (Pliny *NH* 36.65-66; Eichholz, 1962: 149-155).

Most of the Roman glass production seems to be following a standard recipe between the 1st and 4th century CE with specific ratios for each component of the glass. The weight percentage of silica (silicon dioxide) is 60-70%, soda (sodium oxide) is 13-20 % and lime (calcium oxide) being around 5-10% (Henderson, 2013, Rassumen, 2012, Artioli, 2012). There are slight variations between the glass made during this period due to the level of experimentation in a time of transition between the Hellenistic period, Roman period, and the early Byzantine period. There are other impurities which are a part of the sand being used, colourants and decolourizers that are added to the glass which normally make up only 1% of the glass. This is the typical formulation which is also described in Pliny's *Naturalis Historia*. Other notable glass compositions during this time include the Levantine type and HIMT which are described below, showing the major chemical signatures and their alkali source.

Table 3.12. Major compositional groups of archaeological and historic silica-based glass. Modified from Sayre and Smith (1961) and Henderson (2000, 2001). The significant chemical signatures distinctive of the group are in bold.

Glass type	Chemical signature (oxide wt%)					Note	Alkali source
	Na_2O	K_2O	MgO	CaO	Other		
HMG	8–20	**0–3**	**2–10**	3–10		**High-Mg glass** – Near East (1500–800 BC)	plant ash
LMHK	0–8	**4–18**	**0–1**	0–4		**Low-Mg High-K glass** – Europe (Bronze Age)	plant ash
LMG (SLS)	13–20	**0–1**	**0–1**	5–10	0–1 Fe_2O_3 0–2 MnO	**Low-Mg glass** – Near East (after 800 BC) and standard Roman-type **soda-lime silica** glass (AD 50–300)	natron salts
HIMT	16–20	**0–1**	**1–2**	5–9	**1–3** Fe_2O_3 **1–3** MnO **0–1** TiO_2	**High-Fe-Mn-Ti glass** – Mediterranean area and North-Western provinces (AD 300–500)	natron salts
LEG	10–15	**0–1**	**0–1**	8–12	**1–3** Al_2O_3	**Levantine-type** – near East, Mediterranean area, North-Western provinces (AD 500–800)	natron salts
HSB	15–21	**0–1**	**0–1**	4–6	**0–2** Sb_2O_3	**High-Sb glass** – Near East, Mediterranean area (AD 100–300)	natron salts
HKEG	0–14	**2–14**	0–5	6–20		**High-K Medieval glass** – Europe (stained window glass)	plant ash
HLEG	0–1	**3–10**	1–3	4–16	**20–65** PbO	**High-Pb Medieval glass** – Europe	plant ash
HMEIG	10–18	1–3	**3–7**	6–12	**0–1** MnO	**High-Mg Early Islamic** glass (AD 840–1000)	natron/ plant ash
HLIG	8–10	0–2	0–1	4–5	**30–40** PbO	**High-Pb Islamic** glass (AD 1000–1400)	natron/ plant ash
HLHB	2–7	0–4	0–1	0–3	**15–40** PbO **5–15** BaO	**High-Pb High-Ba glass** – China (Han Dynasty 206 BC – AD 221)	witherite?
HAG	3–12	**4–16**	1–2	2–6	**2–4** Al_2O_3	**High-Al glass** – India (1st millennium AD) – maybe several groups	plant ash
FDV	12–15	2–4	1–3	4–10		**Venetian "cristallo"** and **Dutch "façon de Venise"** (16th–17th century)	soda-rich ash

Figure 4: Major compositional groups of historical glasses. Artioli.

Another glass composition which should be noted is the high iron, manganese, and titanium glass composition, also known as HIMT glass, which was popular in the Mediterranean area and the northern provinces around 300-500 CE during the Roman occupation of these areas. This type of glass may have up to 1-2% of magnesium oxide, 1-3 % manganese oxides, 1-3% iron oxides, and up to 1% titanium oxides present in the core of the glass (Henderson, Rassumen, Artioli). This type of glass arrives out of experimentation with natron sources throughout the Mediterranean coastal regions, alongside the advancements in the fourth century glass technology with vessel formation and decoration

that involved a quicker and simpler single process (Henderson, 2013, 96). This will come into play as the context in which these samples were found are thought to be from the 4th century CE layer of occupation at the archaeological site of Stobi.

1.4. Glass corrosion

There are various types of corrosion that can be present on glass depending on the context in which they are found, the composition of the glass etc. The focus of this section will be on burial environment when glass is intentionally buried with the deceased as an offering or gift or as a result of the abandonment of a site or a dump pit, as with the case of the tesserae discussed in this thesis. The main threat to buried glass is groundwater and acidity of the soil in the area causing an ion exchange between the glass and soil (Pollard, 1996, 187). This causes the diffusion of hydrated silica, alkalis, and alkaline earths out into the groundwater, exceed solubility due to pH changes and precipitate as some form of hydrated, crystalline, silicate or aluminosilicate mineral (Pollard, 1996, 187). This is a cyclic process, so it causes the lamellar structure or flakiness that is seen in the corrosion products of buried glass. However, this is a corrosion process that is very dependant on the context condition and so morphologies of weathering crusts such as parallel layers and zigzag banding should only been seen with this environment (Pollard, 1996, 187). The reaction that takes place between the groundwater, soil, and object is not fully understood and it also depends on the concentration of elements that exist in the groundwater and soil, which is why this type of corrosion, its extent and composition, is hard to predict. This is commonly known as de-alkalization when components of glass are leached out from the network due to the surrounding environment. This is an exchange of alkali ions between the glass and the surrounding environment as mentioned above and can be seen in figure 5 below describing the initial stages of the formation of the corrosion layer.

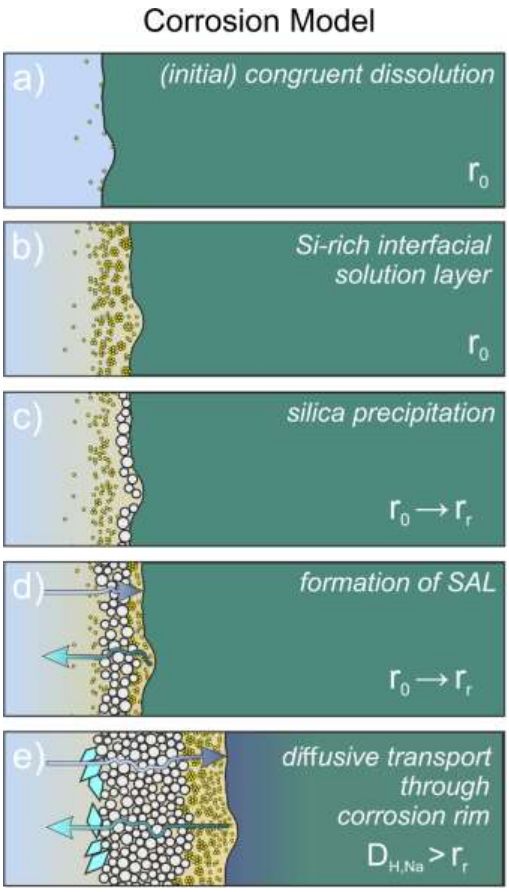

Figure 5: Corrosion model for surface alteration of glass. Lenting et al., pg. 7.

Sandra Davison's *Conservation and Restoration of Glass* (2003) also describes de-alkalization of the glass matrix along with the ion exchange and interactions that take place during burial conditions and the results physical manifestations that occur from these chemical interactions which can be seen in figure 6 below

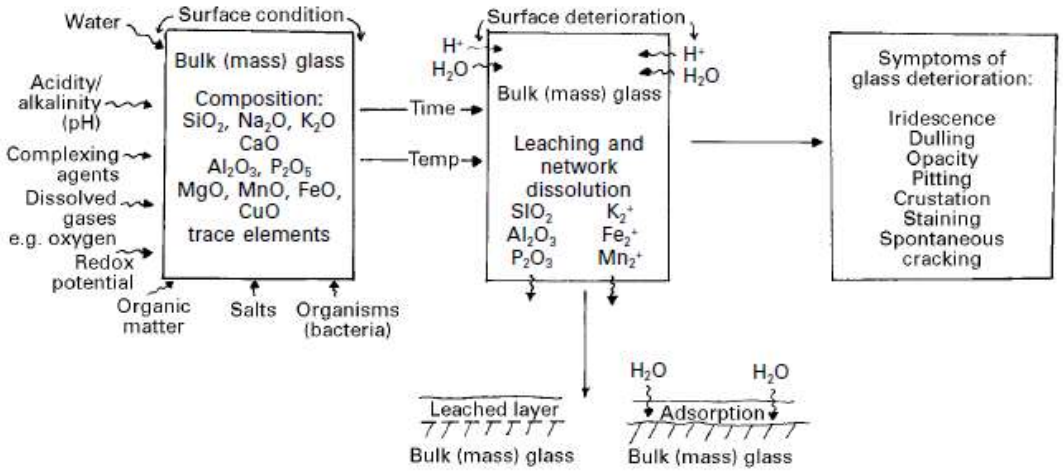

Figure 6: Process of glass deterioration. Davison, 2003, Pg. 174

De-vitrification occurs when the surface of the glass becomes crystalline through absorption of moisture from the environment, creating carbonates of potassium and sodium on the surface which is seen as a white cloudy haze on the surface of the glass (AIC Conservation Wiki, 2019). This can be further corroded into a milky or enamel like surface that flakes and can darken over time which is different from manganese browning. This milky type of corrosion can flake away in "stones" which can leave pits behind on the original surface of the glass or pitted on the corrosion layers. De-vitrification is not to be confused with de-alkalization which can cause a different corrosion pattern such as flaking and iridescence.

Iridescence is another corrosion phenomenon that cannot be removed from the glass, as it is a result of the visual effects from de-alkalization. The iridescence seen on glass is a rainbow-like pattern on the surface of the glass, sometimes associated with other types of weathering patterns or on its own (Davidson, 2003, 183). The intensity of this type of corrosion is dependent on the thickness of the glass corrosion layers it is associated with or if it stands alone. The intensity has to do with the interplay between the amount of metal oxides present, the thickness, and number of corrosion layers present on the glass which refracts light to create this rainbow effect of vivid colours such as pink, purple and gold (Davidson, 2003, 183). This effect is common in Roman type glass due to colourants added in many of the glasses as well as the source materials containing aluminum, calcium, and iron. The iridescent layers as seen under SEM -EDS elemental mapping show the calcium leached and redeposited on the surface, with crystalline material near the surface as seen in figure below (Bellendorf et al., 2010, 138). This supports the interaction between light and layers of corrosion leading to the rainbow colours of iridescence.

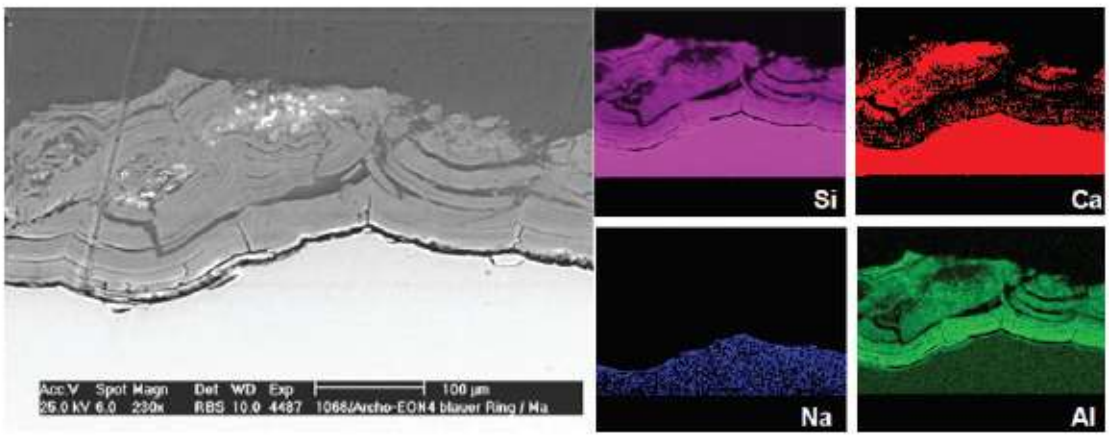

Figure 7: SEM elemental map of Celtic glass ring excavated from early mediaeval site, Germany. Bellendorf et al, 2010.

There are physical manifestations of the chemical change in glass corrosion such as iridescence, pitting, strain cracking, and dulling (AIC Conservation Wiki, 2019) These physical corrosion patterns are important to understand because they contribute to the breakdown and subsequent corrosion of the glass network. The strain cracking appears as a small network of cracks, also known as crizzling, that is distributed in all directions until the glass takes on a sugary appearance due to the high amount of cracking and the entire structure eventually disintegrates. This could be due to the hydrated gel layer which changes with moisture content leading to the formation of these microscopic surface cracks allowing for further moisture to enter the glass matrix (Davidson, 2003, 184). This phenomenon creates a faded or dull appearance in the glass which cannot be restored.

1.5. Previous studies in glass mosaic tesserae

The most recent studies in glass tesserae involve the use of a variety of analytical techniques including X-Ray Diffraction (XRD), Raman Spectroscopy, X-Ray Photoelectron Spectroscopy (XPS), X-Ray Fluorescence (XRF), and Scanning Electron Microscopy (SEM) to look at the composition of the core glass (Artioli, 2012, Arletti et al, 2006, Croveri et al, 2010). There are also studies done on the chemical phenomenon of corrosion that takes place when glass is exposed to different environments such as high relative humidity and temperature, burial, waterlogged and dry conditions. The focus of this section will be on studies done in compositional analysis and corrosion studies of glass mosaic tesserae made in the Roman period throughout the Mediterranean region. This will give a better understanding of the current theories on the relation between composition and corrosion of Roman glass and the analytical techniques employed to better understand this relationship.

Glass mosaic tesserae found at Pompeii, published in 2006, used Electron Microprobe Analysis (EMPA), Scanning Electron Microscopy, and X-ray Powder Diffraction to determine the chemical composition of major and minor elements of the tesserae as well as the crystalline phases dispersed throughout the glass matrix (Arletti et al, 2006, 28). The study revealed that the blue tesserae were heterogenous mixtures of two different phases, one that is rich in Cu, Ca, and Si and another rich in quartz, suggesting it was a fragment of a pigment, commonly known as Egyptian blue, rather than glass (Arletti et al, 2006, 28). The other two blue glass tesserae correlated to typical Roman soda lime silica glass types found between the 1st and 4th century, using copper and cobalt for the light blue and dark blue colours, respectively. The study concluded that the tesserae analyzed supported the archaeological dating of the layer in which they were found.

A study done on glass tesserae of varying colours dating to the 4th century CE found in the Villa del Casale near Piazza Armerina was done by Croveri, Fragala et al. (2010) to determine the corrosion processes that were occurring in the glass. Optical microscopy and SEM were employed to give information about the porosity of the glass, characterise the crystalline areas and surface alteration layers. SEM, XPS, XRF and UV-VIS-IR were used to obtain chemical composition of the tesserae and XRD was used to identify any opacifiers. The study concluded that the glasses that were analysed belong to two main categories of glass which were silica-soda lime glass and silica-soda-lime lead oxide glass (Croveri et al, 934). Overall, the tesserae that showed the greatest degree of corrosion due to the exposure of their surface to external aggressive agents such as biological attack, air pollution, sunlight exposure and the microclimate of the villa itself, were those of the pale blue hue. The compositional homogeneity of the samples overall suggest that the mosaic tesserae have been fabricated in a single glassmaking workshop by an expert craftsman (Croveri et al, 934).

A study published in 2017 investigated glass mosaic tesserae found at basilicas dating to the 5th and 6th century CE in Albania which were similar in colour to the ones used in this thesis research project (Vataj, Civici, et al, 3). The study involved the investigation of 72 opaque glass tesserae from three early Christian basilicas in Elbasan, Byllis, located in central Albania, and Lin, located on the shore of Ohrid Lake. The qualitative analytical tools used were colourimetry and optical microscopy while the quantitative analytical tools used were SEM-EDX, Micro-Raman Spectroscopy and Micro-X-ray Fluorescence to investigate both the macroscopic composition and the microstructure of the samples. Results from this study found that the analysis of the glass composition supported the archaeological dating of the basilicas as well as the use of imported materials from other Mediterranean sites for the manufacture of the tesserae (Vataj, Civici, et al, 13).

Sarah Maltoni and Alberta Silvestri (2018) conducted a study on another 4th century mosaic of the Casa delle Bestie Ferite in Aquileia, Italy which utilized optical microscopy, SEM, XRD and Electron Microprobe Analysis (EPMA) analysis to understand glass tesserae composition during this transition period as described in the previous section between different glass making techniques of the north western provinces and provinces around the Mediterranean sea. The conclusion of this study indicated that MgO and K_2O have contents of both oxides below 1.5 wt % indicating that natron was used as a flux in accordance with the Roman and late antique tradition (Maltoni, Silvestri, 421). There is also a level of technological variety that is seen in the mosaic that was analysed which mirrors the political,

economic and cultural complexity of the 4th century CE which is confirmed to be a period of transition between the Roman and early Christian Byzantine period (Maltoni, Silvestri, 428).

This is significant to note as the mosaic tesserae that are analyzed in this paper are assumed to be dated to the 4th century CE based on archaeological evidence, through the context and layer in which these tesserae were found. This study will help in understanding the glass used for the creation of the wall mosaics in the complex around the Temple of Isis at the archaeological site of Stobi. The decision to use the following experimental was based on previous studies done on corrosion analysis while being mindful of time considerations and access to analytical equipment.

2. Historical Background of Stobi

2.1. Macedonia

Macedonia stems from the ancient Greek word “makednos” which means “a tall one” or a “highlander” and believed to have arisen from the area of Boeotia (Homeric Emathia) where the Argeads established their kingdom. Later, the name was applied to match the larger area of the ancient Macedonian Kingdom that was established and expanded by Philip II of Macedon, reached its greatest extent under Alexander III, eventually fell into the hands of the Romans after the defeat of Perseus, the last king of the Antigonid empire in 168 BCE. Most of the primary evidence for the socio-political and cultural economy of the Macedonian Kingdom is from Greek historian Polybius, writing in detail of the events during 264-146 BCE, and later the Roman historian Livy, who was active in the 1st century BCE. Today, most of the geographical region of Macedonia is included in the modern countries of Greece, North Macedonia, and Bulgaria.

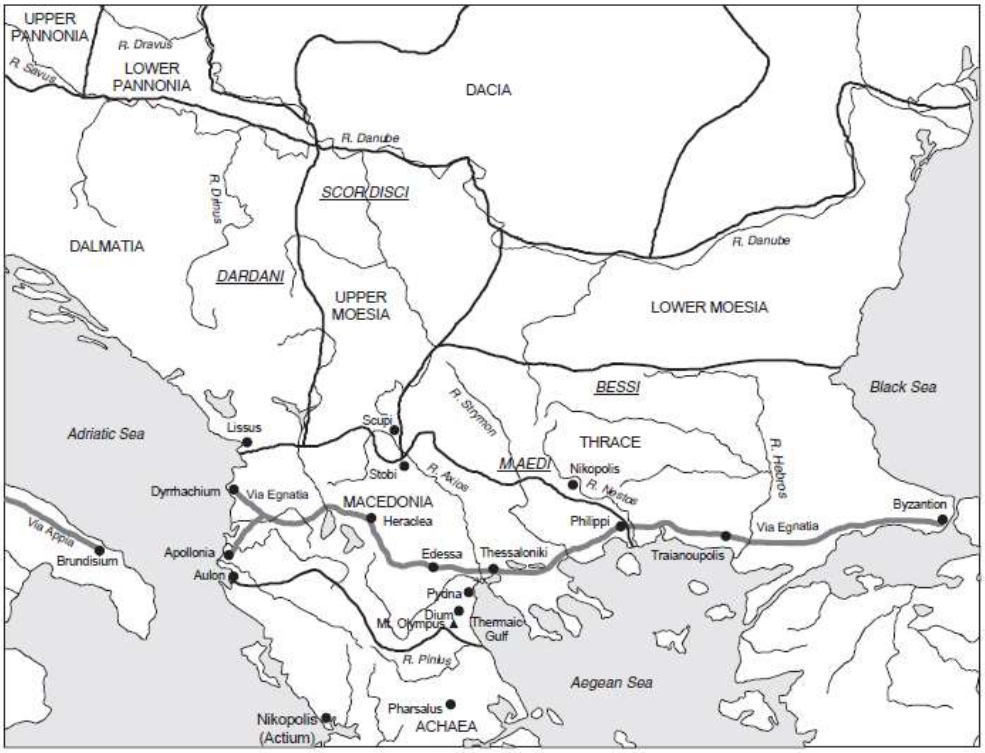

Figure 8: approximate boundaries of the Roman province of Macedonia, 147 BCE. Pg. XXIV. Ancient Macedonia, Ian Worthington.

2.1.I Terminology

The term Macedonia will be used in this paper to define the historical geographical area at time. If the term refers to the area of modern northern Greece with the same name, a clear specification will be provided. North Macedonia will be used to define the modern country and area in which the site lies. Other definitions and acronyms will be defined as they appear throughout the text.

2.2. History of Stobi

The archaeological site of Stobi lies at the confluence of the Vardar and Crna River in central portion of present-day North Macedonia. Earliest evidence of human occupation of the area dates to the late 3rd century BCE in the form of grave goods found in the graves as there is no intact Hellenistic sculptures or inscriptions (Sokolovska, 1975, 135). The town underwent expansions and was a prosperous community up until its abandonment in the late 6th century CE. The city of Stobi is first mentioned in Livy's *Ad Urbe Condita,* in which he speaks of the place where Philip V was victorious over the Dardanians in 197 BCE. "[Phillip] quickly levied troops in the cities of Macedonia and with six thousand infantry and five hundred cavalry suddenly fell upon the enemy near Stobi in Paeonia." (Liv, 33, 19) It is thought that Phillip V of Macedon annexed the town along with Paeonia in 217 BCE during

his campaign against the Dardanians and since this moment, Stobi and Paeonia became a part of Phillip's Macedonia. After the fall of the Antigonid empire, the region of Macedonia was split into four independent merides known as Amphipolis, Thessalonica, Pella and Pelagonia. The contact between these merides was controlled by the senate and Stobi entered the area of Pelagonia.

Notable events for the ancient city of Stobi include being a salt emporium for the third meris of Macedonia in 167 BCE which allowed for the economic flourishing of the city as described in Livy's accounts of the city. In 147 BCE, Stobi became a part of the newly established province of Macedonia, however, due to poor archaeological data and the later development of the site, it is hard to determine the boundaries of the northern part of the province. In the 69 CE, the city became a municipium under the emperor and began minting its own coins with the name "MUNICIPUM STOBENSIUM" seen in Figure 8 below. In the mid 5th century CE, the new episcopal basilica was built above the earlier church and a Christian church replaced the synagogue on site, signalling Christianity as becoming the dominant religion for Stobi and the rest of the Roman Empire in the 4th and 5th century.

Figure 9: Roman Provincial Coin. Titus and Domitian as Caesars, 69-70 CE. T CAESAR IMP DOMITIANVS CAESAR, head of Titus with laurel wreath l. and the Domitian r. towards each other. Rev: MVNICIPIVM STOBENSIVM, tetrastyle front of a podium temple with a cult statue

At the beginning of the 4th century CE, Stobi underwent new urban development with many residential and public buildings and in the same century Christians were granted religious freedom in 313 CE. The first bishop at Stobi is recorded at the Council of Nicea in 325 CE, with the oldest church at Stobi dated to the end of the 4th century and is adorned with wall paintings and mosaic pavement (Wiseman, 1975). A notable event for Stobi history is when Theodosius I visited the city in 388 CE and during his stay, he issued two edits concerning religious affairs (Wiseman, 1986, 41). He was thought to stay at a luxurious home

that was near the Episcopal Basilica and henceforth the extravagant room has been referred to as the Theodosian Palace as seen in Figure 9 below. During the 4th and 5th centuries, magnificent Christian basilicas were built in every large town, which explains the construction of the basilica on top of the synagogue at Stobi and the construction of a Christian mosaic floor in the House of Polycharmos (Wiseman, 1986, 40). There were six more basilicas constructed in the city during the 4th and 5th centuries which points to the power and wealth of the Christian community in Stobi.

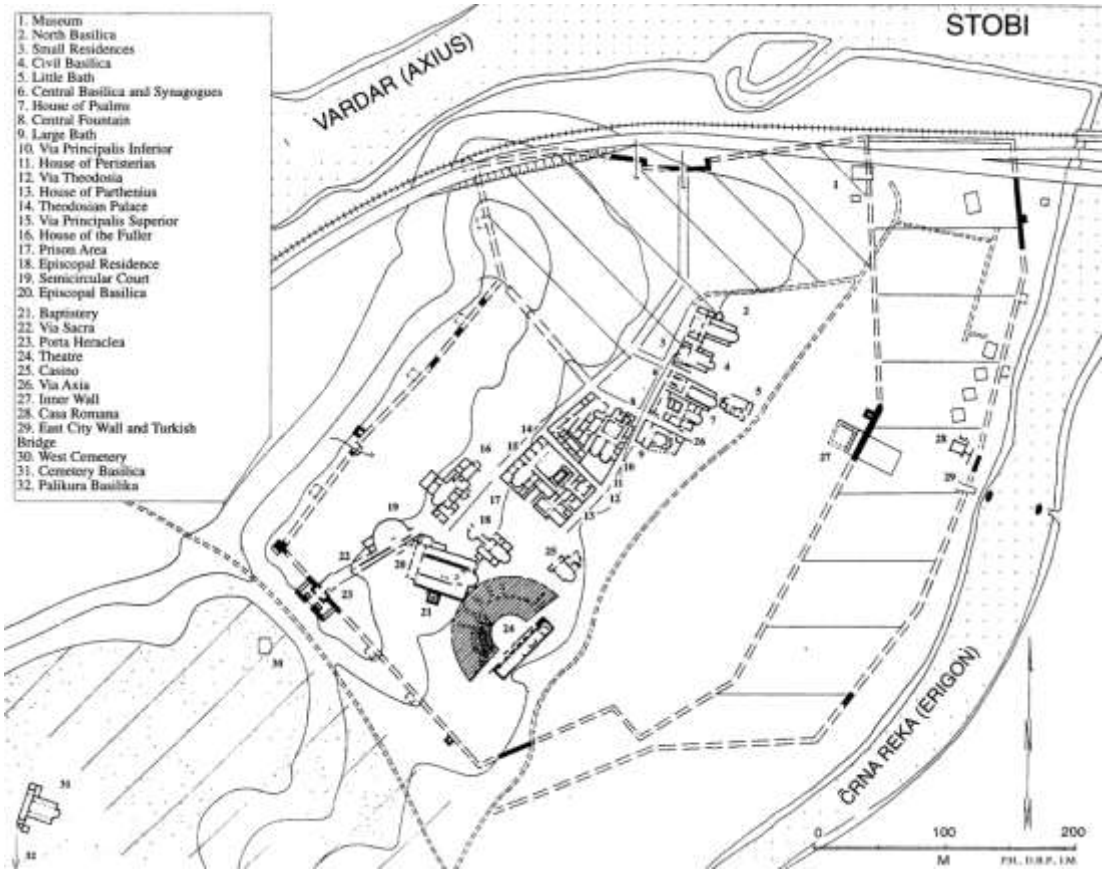

Figure 10: Map of Stobi, "Loca Sanctorum Macedoniae, the cult of martyrs in Macedonia from the 4th to the 9th centuries" (1997) by Blaga Aleksova

At the end of the 3rd century CE, there were significant catastrophes that led to the downfall of Stobi as a city. The first catastrophe was the ravage and pillaging of the Goths and the Heruli in 267 CE across the Balkan region, along with subsequent natural disasters such as an earthquakes, a significant landslide and flooding in the region during the 5th century CE (Wiseman, 1975, 42).The Roman empire went under administrative reform causing the province of Macedonia to be divided into two provinces of Macedonia Prima and Maceondia Salutaris, which was later renamed Macedonia Secunda in the 5th century CE with Stobi as the capital. A larger earthquake shook the city of Stobi and destroyed parts of the

Basilica, Synagogue, and parts of the theatre in the early 6th century CE (Wiseman, 1986, 41). Rebuilding seemed futile after many people fled when their homes were destroyed in the quake while there was a growing fear of the Avars and Slavs travelling south after they finished in the northern regions. There was also the abandonment of the massive theatre due to the destruction caused by the quake as well as the idea that the venue propagated paganism unpopular by the growing Christian religion (Wiseman, 1986, 43). After these various events, the province of Macedonia Secunda was dissolved and in 570 CE, most of the residents evacuated or abandoned the area, based on archaeological evidence.

2.2.I. Archaeological Context

Excavations on the site of Stobi began after WWI, when German, French and Serbian soldiers uncovered parts of the site while digging trenches. The systematic excavations of the site began in the 1920's which was led by the National Museum of Beograd. After WWII, in the period between the 50's and 60's there were minor excavations done by the Archaeological Museum of Skopje. In the 1970's, there was a joint Yugoslav-American project that was sponsored by Boston University, the National Museum of Titov Veles and the University of Texas headed by Djordje Mano-Zissi, James Wiseman and Blaga Aleksova.

The excavations in the 1980's was headed by the National Museum of Titov Veles and halted in 1985 due to rising tensions between ethnic groups in the region and the subsequent Yugoslavian civil war. After 1995, there was the expansion of the main highway which allowed for salvage excavations to take place. This is when 1500 graves were unearthed near the western necropolis and large conservation projects took place in the old and new Episcopal Basilica, building walls, Baptistery, and the Building with the Arches.

Under the direction of Silvana Blaževska, the archaeological site of Stobi became a National Institution under the Ministry of Culture in 2008 and in 2009 site management was given solely to the National Institute Stobi. This allowed for more projects to take place in excavations, conservation, and presentation of the site. In 2008, Jovan Radnjanski coordinated the project of the Temple with Hypogeum and in 2012 the team discovered an impressive marble sculpture with stylistic attributes indicative of the Egyptian goddess of Isis. This allowed for further excavations around the site and conservation of the building to take place for the following years. In 2012, excavations around the Temple of Isis in so called "Room 1" led to the discovery of wall mosaic fragments and subsequent excavations within

the same area the following years led to more than 400 wall mosaic fragments found within the same locus. Below are some examples of these fragments that have been found.

Figure 11: Some of the wall mosaic fragments found near the Temple of Isis. Photo taken by Paige Van Tassel

2.2.II. Mosaics at Stobi

Approximately 1560 square meters of excavated territory at the archaeological site has partly or fully preserved floor mosaics dating between the second to sixth century CE. The mosaics at Stobi are expansive and cover the major centers of business and leisure within the ancient city as well as smaller houses in the living quarters of the city. There is evidence of both floor and wall mosaics with varying degrees of precision work exemplified in certain areas such as in the Episcopal Basilica, the Theodosian Palace, the living quarters, and most recently the rooms around the Temple of Isis. The stylistic variations of geometric, floral, and animal motifs are presented throughout the mosaics using the popular mosaic techniques of opus sectile, opus tessellatum, and opus vermiculatum. These mosaic styles refer to the size of the stones that were used in the creation of mosaic pavements, beginning from the Hellenistic period onwards.

Opus sectile is the most basic form of mosaic pavement construction that uses cut pieces of stone with space no larger than one millimetre between the laid stones to make geometric and floral designs. The stones used are polished slabs which are cut to shape in place rather than using smaller stones to create the shape which allow for a bold definition of lines within the design created by the contrasting colours of the stone. The earliest examples

of these types of pavements are seen in the Near East as early as 3000 BCE with large marble inlays, however, this specific type of pavement refers to the patterns seen in and around Italy during the Roman Republic as early as 2nd century BCE. There are a few examples of this type of mosaic work that are employed in the earlier phases of the Episcopal basilica as seen in figure 11 below which shows the presbytery located in the northern part of the early church during its second phase of reconstruction, using stone pieces that are larger than 30 millimeters.

Figure 12: Second phase of the mosaics in the early church examples of opus sectile in the presbytery. Ruth Kolarik, pg 302.

Opus tessellatum is a technique that developed alongside the production of pebble mosaics in the Hellenistic period. The stones and other materials used in the creation of the mosaic range from five to thirty square millimetres in size. There is no specific transition

period between the use of pebble to cut tesserae, however, during the 3rd century BCE, mosaicists begin experimenting with both pebble and square tesserae, with the full use of regular cut tesserae as pavements in the early 2nd century BCE in the eastern Mediterranean (Dunbabin, 18). This is the predominant style that is employed for the floor and wall mosaic fragments found at the archaeological site of Stobi.

Opus vermiculatum is the most elaborate form of mosaic work with the cut pieces being no larger than 5 mm^2 and is described as "worm-like" because the smaller contours allow for more detailed work. The earliest example is in Greece originating from 200 BCE with a large corpus of this type was found on the island of Delos. There is also evidence of highly specialized work in eastern Mediterranean cities including Pergamon, Ephesos and Alexandria around the same time that Greece is producing similar detailed mosaics (Smirinou et al, 67). The main purpose of this style is to put emphasis on the figures and foreground the details of the work, giving the illusion of space in a two-dimensional work. This is largely seen in emblemata which are the detailed centerpieces of a mosaic work that make up the story or theme of the pavement (Smirinou et al, 67). There are a few examples of this kind of detailed work seen in the floor and wall mosaic fragments found at Stobi such as figure 12 below.

Figure 13: Wall mosaic fragments exhibiting opus tessellatum and opus vermiculatum with stone and glass. Photos taken by Paige Van Tassel

2.2.II.a. Episcopal Basilica

The Episcopal Basilica is the most significant Christian building at Stobi and it has two significant periods in which it was functioning as a Christian basilica. The first period is related to the Old Episcopal Basilica which was built in the middle of the 4th century CE, built by the Bishop Budius and has a three-aisle concept. The second period of the basilica

has significant reconstructions and expansions that took place in the second half of the 4th century. In Ruth Kolarik's report on technical observations of the floor mosaics at Stobi, she mentions the extensive and complex layers of floor mosaics found in the original and expanded Episcopal Basilica. There is evidence of blue-green, gold, and black glass paste tesserae used in the wall mosaic fragments which were found in the apse of the first phase of the building (Kolarik, 1975, 106). Figures 13 and 14 show a composite image of the floor mosaics in the Episcopal Basilica.

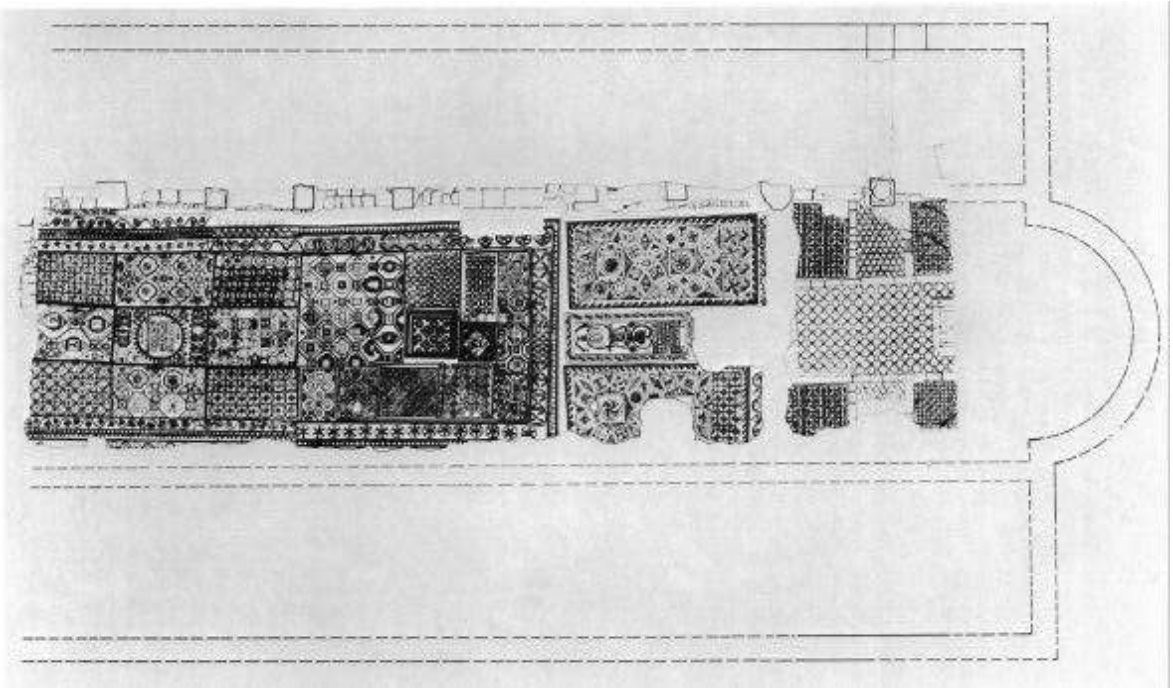

Figure 14: Composite image of the mosaics in the Episcopal Basilica after Aleksova "Basilicas". Ruth Kolarik, pg. 298.

Figure 15: Floor mosaics after conservation and reinstallation in the Episcopal Basilica after January 2015. Image taken from Stobi Facebook webpage. https://www.facebook.com/Stobaeus/photos/a.127592253963716/3044917645564481/?type=3&theater

2.2.II.b Baptistery

The Baptistery is believed to have been constructed around the 5th century CE based on indirect archaeological evidence in the form of pottery and a coin of Arcadius dating from 395-405 CE. The construction of the floor mosaic in the baptistery is limited to six colours

including a white dolomite marble, green, black serpentine, gray limestone, pink brecciated marble, yellow marble, and red orange terracotta (Kolarik, 1975, 85). The stylistic features of the mosaic are similar to those in the House of Psalms, where that floor mosaic has more precision in its execution and detail due to the smaller sized tesserae, suggesting that these mosaics derive from the same school. There is no evidence to suggest that this mosaic had used glass tesserae however it is mentioned in this thesis to show the range of stylistic mosaics found at the archaeological site of Stobi. Below is an image of the baptistery mosaic from above with the recently conserved columns and kantharos in place.

Figure 16: Baptistery. Archaeological Site Stobi. Taken from Facebook webpage. https://www.facebook.com/Stobaeus/photos/a.127592253963716/3138924939497084/?type=3&theater

2.2.II.c. Temple of Isis

The temple was discovered in 2008 at the lowest terrace of the ancient city of Stobi between the theatre and the southeast fortification wall. The following year, excavations revealed a larger complex around the temple and in 2012, a marble sculpture of the Egyptian goddess Isis was discovered, confirming the dedication of the temple to the goddess (Blazevska, Radnjanski, 2013). Based on the archaeological evidence, the temple was built in the first half of the 2nd century CE and destroyed in the last decade of the 5th century CE. During the 6th century, the whole complex was rebuilt to accommodate the needs of the residential area of Stobi and later the whole city was abandoned in the last decade of the 6th

century CE (Blazevska, Radnjanski, 2013). In this report, there is mention of floor and wall mosaics excavated from fill deposits around the temple, however, it is unclear in which building these wall mosaics once belonged.

Figure 17: Temple of Isis after conservation, 2012. Photo taken from Jovan Radnjanski and Silvana Blazkeva, The Temple of Isis in Stobi, pg. 242.

2.2.III. Materials of Construction

There are different methods of construction for a floor and a wall mosaic where one is more robust to endure being walked upon and the other is similar to layers made in preparing a fresco wall decoration. The construction of a floor mosaic has five preparation layers before the tesserae are laid into the mortar known as the support, intermediate layers, and the pavement which is described in the Architecture of Vitruvius, *De Architectura,* written in the 1st century B.C. The main support layer is the statumen, the intermediate layers are the rudus and nucleaus, while the final decorative layers that are seen with the naked eye are the bedding layer and tesserae (Caldeira, et al, 2019, 4). The statumen is laid to protect the soil and mosaic from depressing into the ground and it is normally composed of large boulders atop the natural soil. The rudus is composed of a mixture of crushed stone and the natural soil used to even out the surface in preparation for the nucleus (Caldeira, et al, 2019, 4). The nucleus is composed of smaller crushed stone, usually finer than the rudus layer, and is there to help set the mortar in place. The bedding layer is usually composed of the mortar and is laid just before the tesserae are inserted which means that the mosaicists must work within a

day, sometimes within hours before the mortar sets (Caldeira, et al, 2019, 4). Below is a drawing of the stratigraphy of layers that lay beneath a mosaic pavement.

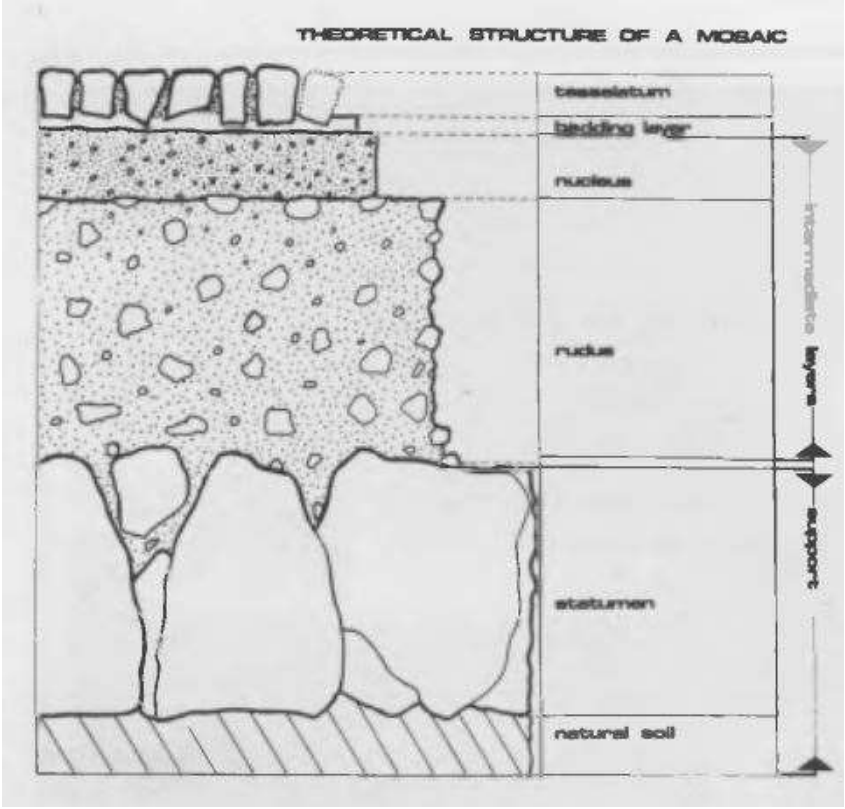

Figure 18: Theoretical structures of a mosaic. ICCROM International Symposium on the Conservation of Mosaics. 1977

The layers that compose a wall mosaic are like those of a fresco, however, vary slightly based on the force and load applied on a wall mosaic decoration as opposed to a floor pavement. The archaeological site of Stobi has some examples of fresco and wall stucco decoration dating to the late Roman and early Byzantine period which were analysed by Wiseman and Geogievski. Their research was conducted on several fresco and wall stucco fragments chosen from ten locations throughout the site such as the House of the Fuller, the Synagogue, the central Basilica, the Casa Romana, and various structures near and in the Episcopal Basilica (Wiseman, 1975, 164). The findings for this research showed that most of the fragments that were analyzed from different buildings throughout the site had the same construction technique with small variations in the percentage of lime, sand, clay and the most common temper being straw and crushed brick to provide better insulation and strength. The pigments found on the fresco and wall stucco fragments were also analyzed and found to be gypsum white, charcoal black, iron oxide red, chalk, raw sienna, green earth with a mixture of the mentioned pigments to create pink and grey colours (Wiseman, 1975, 183).

Evidence of these pigments in the preparatory layers of the wall mosaic fragments can be seen in the next section.

2.2.III.a. Wall Mosaic Fragments

Previous studies on wall mosaic fragments at the archaeological site of Stobi have been completed by Ruth Kolarik in her report on the technical observations of mosaics which a brief section on wall mosaic fragments that were found in the Episcopal Basilica. She mentions the report by R. Egger and the discovery of similar wall mosaics found throughout Macedonia (Kolarik, 1975, 105). She also notes the discovery of colorful stone and glass tesserae, gold leaf tesserae, and blue-green glass paste tesserae found in the apse of the Episcopal Basilica which were set at different angles so the light would catch and reflect, giving a shimmering effect to the mosaic. The admixture of straw found on the mortar backing of the fragments proves that these fragments found were wall mosaics, separate from floor mosaics.

The wall mosaic fragments in question are a group of around 162 fragments that were conserved in the summer of 2018 and are a part of a larger group of fragments held in on-site storage under the collection name “M3-12-01”. This collection of wall mosaic fragments collectively forms more than 400 fragments that were found in this area surrounding the temple of Isis. A number of these fragments have evidence of a fresco style sketch layer that was used to guide the mosaicist in creating the design of the mosaic. Below is evidence of the base layer sketch, using presumably an iron oxide red which has been used in the creation of frescos and wall stucco in other buildings on site.

Figure 19: Evidence of a base layer sketch as seen by the red paint on the mortar at the bottom of the fragment on the left and throughout the base of the fragment on the right. Photos taken by Paige Van Tassel.

2.2.III.b. Glass

Kolarik mentions the use of black and blue green glass paste tesserae used for wall mosaic fragments in the Episcopal Basilica as well as evidence of glass in the floor mosaics found in the same complex (Kolarik, 1975, 69). The wall mosaic fragments found near the Temple of Isis, which are the focus of this report, suggest the use of a variety of coloured glass to create a lavishly decorated figure as some fragments use smaller *opus tessalatum* that is normally cut to sizes less than 1 cm for detailed figural depictions. This technique is employed in both stone and glass to allow for a more realistic figural depiction. On some of the wall fragments associated within the same context of the glass tesserae purple and blue-green glass is used as seen in figure 20 below.

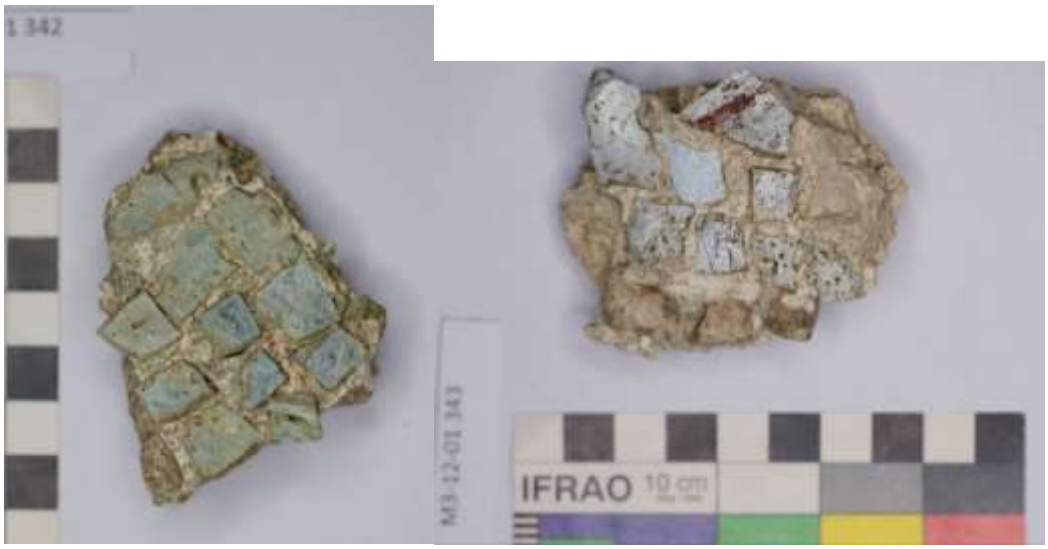

Figure 20: M3-12-01 342 wall mosaic fragment on the left with primarily green – blue glass tesserae. Photo taken by Paige Van Tassel. M3-12-01 343 wall mosaic fragment will mainly glass tesserae and a few marble tesserae near the bottom of the fragment.

2.2.III.c. Stone

The stones used for the mosaics at Stobi are locally sourced from quarries in the area. The stones used encompass a variety of colours that are displayed in the mosaics including glass tesserae that is mentioned above to create figural and geometric pavements. The stones used include yellow and red ochre, pink and red andesite, green serpentine, green cipolin, hard green silicate, white marble – both calcite and dolomite, gray-black and beige limestone, and red-orange terracotta. These are just a few of the stones that are mentioned in Ruth Kolarik's technical observations of the floor mosaics done in 1975 and have been mentioned in her brief appendix on wall mosaics.

2.2.III.d. Mortar

The recipe for mortar used in floor and wall mosaics vary due to the force and load difference between the floor and wall. The traditional recipe that is used to create mortar for floor mosaics include the use of limestone which is crushed and burned in a kiln to create quicklime, CaO, an aggregate such as gravel or sand, sometimes brick to add to the bulk, and water. As the mortar fixes to the base and "sets", CO_2 is reabsorbed from the atmosphere converting back into $CaCO_3$ with a crystal size of 1 micron or less (Folk, Valastro, 30).

Wall mosaics use a lighter recipe for creating mortar which is similar to the creation of frescos to prevent slumping or collapsing over the years. There are two types of fresco that can be applied to a support wall, buon fresco and fresco secco. The more common one being fresco secco as the artist is not limited by the drying plaster, whereas buon fresco works within the drying time frame of the plaster. The frescos at Stobi employ the secco technique as well as the molded stucco technique, and therefore it is assumed that the similar type of fresco technique was employed when creating the sketches or preparatory layer for the wall mosaics (Wiseman, 1975, 184). However, there was a notable change in the source of lime or change in tradition from carbonate limestone to dolomitic limestone or marble during the 4th to 6th centuries based on previous studies on fresco fragments found throughout Stobi (Wiseman, 1975, 185). Based on these studies, a similar type of limestone was used for the fine white plaster which can be seen in Figure 21 below to create the wall mosaics.

Figure 21: Underside of a wall mosaic fragment showing different layers, with the more fine white plaster seen at the bottom right side of this image. Photo taken by Paige Van Tassel.

2.3. Evidence of glass use at Stobi

There is a wide variety of material evidence that has been excavated from Stobi since excavations began in the 1920's. This evidence serves as a visual example of how the site developed with the changing technologies of glass making in the 1st century CE. There is evidence of a glassmaking workshop, which include glass rods and ingots as well as dump sites for scraps that were discarded after making the glass tesserae (Wiseman, 1978, 398, Radnjanski, Nikolovski, pers.comm. 2019). However, no kiln has been found on the site to date which suggests that there may have been a secondary glass making workshop where the glass was imported to the city and then re-worked at the studio to be sold for local consumption. Below are a few examples of the shift between the core formed glass, free blown glass to mold blown to create a thin profile of the glass.

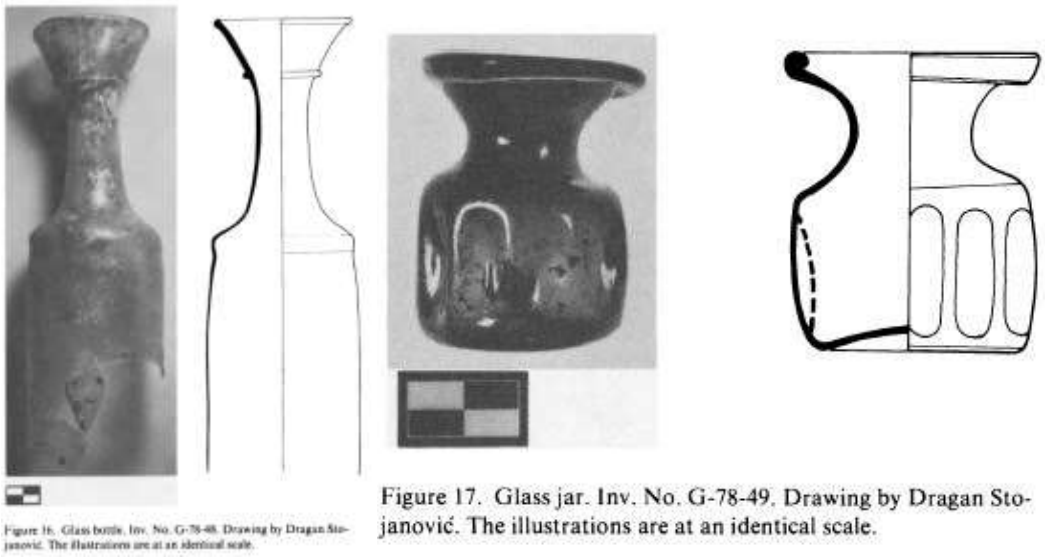

janović. The illustrations are at an identical scale.

Figure 22: Examples of glass found during excavation in 1970's. Drawings by Dragan Stojanovic. Wiseman, 1978.

Figure 23: Examples from National Institute Stobi website of excavations in 2013.

The material evidence to suggest a glass blowing workshop are glass rods and other items used in the glass working process have been found in the 1970's and onwards in the excavations by the joint Yugoslav-American project. This would not be uncommon as any large industrial city during the Roman period would have had a secondary glass making workshop not for forming glass but reworking the glass in glass blowing, moulding or cutting glass blocks to make small tesserae (Henderson, 2013, 247). This is largely because the primary source material for making glass existed near the Middle East and Levantine region, so it made more sense to have larger kilns capable of reaching the high degree necessary to melt the silica closer to the source and later shipped out to secondary workshops (Henderson, 2013, 247). The secondary workshop would only need a kiln that can reach a temperature of around 900 degrees Celsius, like a pottery kiln, to melt and rework glass blocks and rods, however, no such kiln has yet been found at Stobi.

2.4 Glass Conservation at Stobi

The conservation of glass and pottery workshop in cooperation with the Balkan Heritage Field School and the National Institute Stobi has hosted students from across the world to participate in the conservation and preservation of glass and pottery found at the archaeological site. During the off season, there is one glass conservator working on site to conserve the numerous glass collections held at the site. The conservator of glass at the archaeological site, Biljana Peeva has been kind enough to supply some imaging of vessels that exhibited similar corrosion behaviour such as iridescence, pitting, and powdering. This type of corrosion is also seen on blue green glass of other vessels found at the site as well as

the blue green glass tesserae that is observed in this report. Figure 24 shows images of the vessel and pitting corrosion under LED magnification.

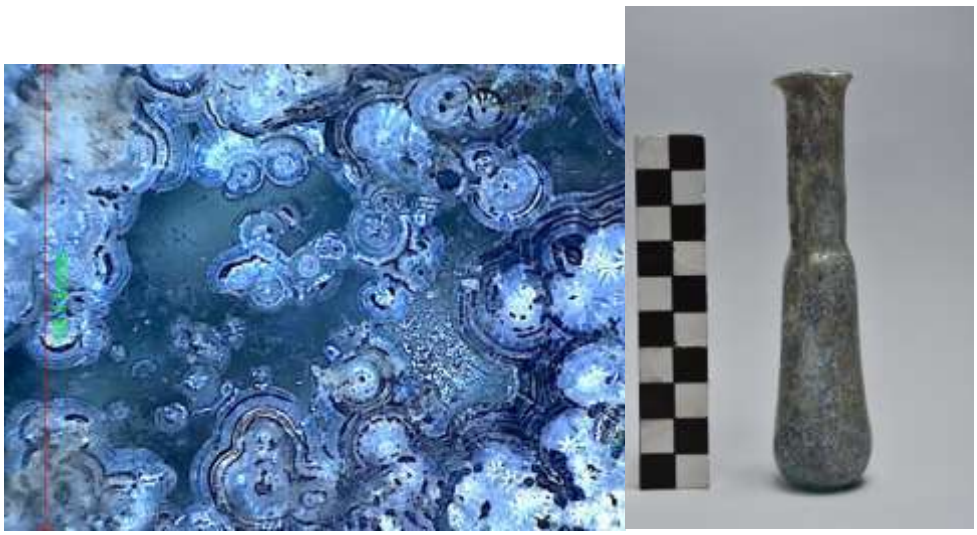

Figure 24: ST-95-82 vessel magnification using DINO lite LED microscope (left) and under normal light to scale (right). Images taken by Biljana Peeva.

Other conservation issues at the archaeological site include the stabilization of the glass tesserae in the wall mosaic fragments. The fragment pictured below, along with several others in the collection, have completely disintegrated and it is unclear on the exact cause of this phenomenon. A large part of the collections is stored on site with improper temperature and relative humidity, along with no pest control in place allowing little critters to walk, defecate, and nibble on the pieces. These fragments were also previously conserved in 2012 with Estel 1000, an ethyl silicate that is often used as a consolidant on weathered silicate materials including stone and glass.

Figure 25: Wall mosaic fragment conserved in 2012, now powdering and deteriorating. Photo taken by Paige Van Tassel.

3. Experimental

3.1 Glass Tesserae

Fourteen glass tesserae were chosen for this project and taken from the complex surrounding the Temple of Isis which is suggested to be dated to the Roman Imperial period and violently destroyed in the 4th or early 5th century CE (Blazevska, Radnjanski, 2015, 216). The glass tesserae were taken from the same archaeological layer. Below is the locus sheet created in 2018 by Kristen Jones and Kristijan Tosheski, students working at the archaeological site of Stobi, showing the archaeological layer of excavations in which the glass tesserae for this project were found. Under локуси (locus) there is a description of each layer that was excavated during that season. E 1.48 describe a group of stones, brick, and materials for construction/building. E1.50 describes a layer of hard compacted brown soil with leftovers of small rocks and mortar. E1. 54 is the floor level of the building with compact soil with small rocks and small fragments of ceramics. The construction materials mentioned in this locus sheet is where most of the wall mosaic fragments were found.

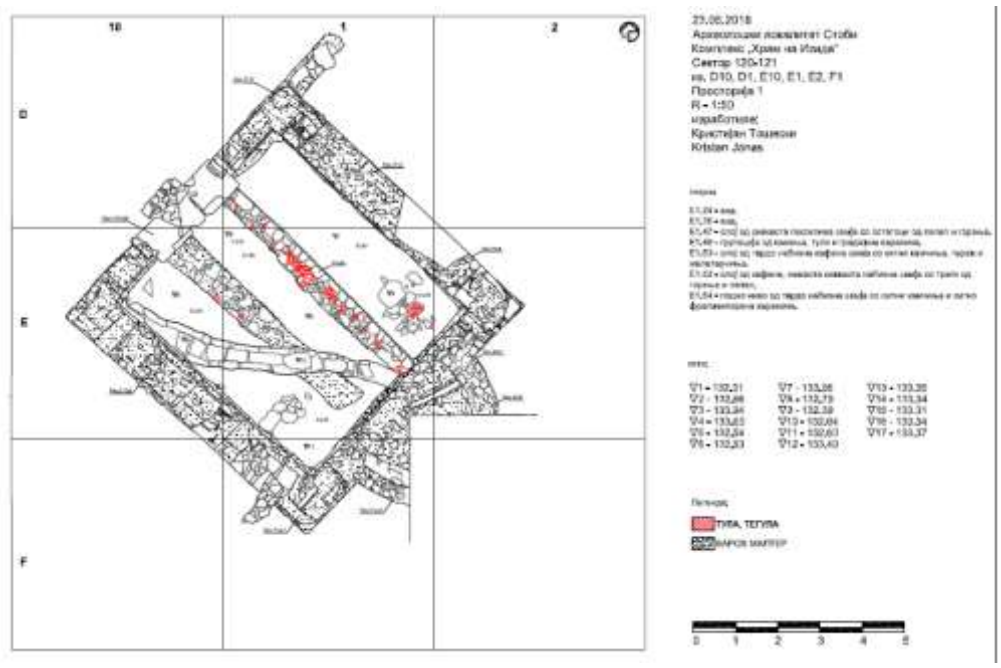

Figure 26: Archaeological layer and locus in which the wall mosaic fragments and tesserae were found. Documentation by Kristen Jones and Kristijan Tosheski.

3.2 Documentation

The glass tesserae were taken from the same archaeological layer where the wall mosaic fragments were found. Half of the samples are blue, and the other half are a green-yellow hue, which have been naturally coloured, and all of which have varying degrees of

corrosion, with one exhibiting little to no iridescence while others have iridescence, pitting, and powdering surface. The samples range in weight from 0.3 grams to 1.8 grams and are no larger than 2 squared centimeters, indicating they were most likely used in opus tessellatum style of mosaic decoration. Most of the samples are cubic in shape while there are two samples that are more triangular. One sample, number 14, has been well preserved, exhibiting little evidence of corrosion on the surface of the glass. Below is a photograph of the relative size of each tesserae chosen for analysis in this report.

Figure 27: Samples used for analysis with their associated number. Photo taken by Paige Van Tassel.

3.3. Instrumentation

The following analytical techniques were chosen to visually and chemically characterize the corrosion products seen on the tesserae and identify the core chemical components of the glass matrix. This was done to see if there is any correlation between the observed patterns seen on the surface corrosion and the chemical composition of the glass and corrosion layers. LED digital microscope and light microscopy were readily available through the Laboratory of Archaeometry, University of the Peloponnese. These techniques offer the ability to see clear details that are not visible with the naked eye. Observations under light microscopy allows for colour detailed magnification of any inclusions or impurities seen in the core glass matrix of the tesserae.

Portable X-Ray Fluorescence was utilized to analyze the corrosion and tesserae intact through quantitative analysis and allow for quick and easy determination of trace elements. Scanning Electron Microscopy was utilized to offer semi-quantification of the core glass composition using spot analysis and further observation of the corrosion layers through line

scans and secondary electron imaging. SEM also allows for analysis of the lighter elements, such as sodium and magnesium, which are important chemical signatures used to understand the different types of glass composition. These techniques were carried out at the University of the Peloponnese's Lab of Archaeometry and thus could be analysed by the author. More advanced techniques that were available at the NSCR Demokritos, such as X-ray photoelectron spectroscopy (XPS) which allows for further chemical characterization of the glass corrosion products, were considered however decided against due to the time constraints and limitations of this project.

3.3.I. Sample Preparation

Each sample was cleaned with ethanol before being embedded in resin. Each sample was cast using Bioplastic Casting Resin and Catalyst in silicon square trays. The samples were then split with a Buehler IsoMet Low Speed cutting machine and silicon carbide saw. The resulting thick sections were then polished with mineral spirits 3M silicon carbide sandpaper up to 2000 grit so that the glass samples could be observed under reflected light microscopy.

Figure 28: Glass samples embedded in casting resin to create cross sections. Photo by Paige Van Tassel

3.3. II.LED Digital Microscope

Visual analysis of the glass samples was done using a fibre optics system (FOM/i-scope, Moritex). The images taken were in JPEG format and at 5x and 10x magnifications to visually characterize the surface corrosion patterns seen on the tesserae.

3.3.III. Reflected Light Microscopy

Visual analysis of the colour, corrosion layers, and other impurities within the glass core was done with an Olympus BX51 (or BX53) microscope with fiber optic (Zeiss KL

1500 LCD) lamps for reflected light. Olympus DP72 camera was used to capture images along with OLYMPUS Stream imaging software for image processing.

3.3. IV. Portable X-ray Fluorescence

Non-destructive portable X-Ray Fluorescence (pXRF) analysis was applied on all samples using a portable Bruker Tracer III SD set up, with a beam diameter of 3 mm done at the University of the Peloponnese Laboratory of Archaeometry. Analysis was done prior to embedding the samples in resin and corrosion left intact on the surface of the samples. All samples were cleaned with ethanol prior to analysis to remove any impurities from the surface of the samples. Each sample was analysed three times on different surface areas of the tesserae to ensure accurate statistical data.

Data quantification was made using S1PXRF software and a custom-built calibration curve, created in collaboration with the scientific personnel of Bruker. The calibration curve was based on the existing file for ceramics, which was then updated based on the measurements of glass standards (1412, NIST610, NIST612, NIST620) through fundamental parameters which are outlined in "Studying a Funerary Roman Vessel Glass Collection from Patras, Greece: An Interdisciplinary Characterization and Use Study" (Palamara, Zacharias et al., 2016). All data results have been normalized to 100%.

3.3.V. Scanning Electron Microscopy – Electron Dispersion Spectroscopy

The polished samples were analyzed under a SEM type JEOL JSM-6510LV coupled with an Oxford Instruments EDS. The analytical data were obtained by INKA software. The bulk analyses were conducted at high vacuum, 20 kV accelerating voltage and with a count time of 300 seconds. This was done to ensure precision and accuracy in the results and the process for this technique is outlined in "Studying a Funerary Roman Vessel Glass Collection from Patras, Greece: An Interdisciplinary Characterization and Use Study" (Palamara, Zacharias et al., 2016). Each sample was measured three times on different areas of the core glass cross section for statistical purposes. Line scans were completed on each sample to further understand the chemical composition from core glass to the corrosion layers. This analysis was two-fold in terms of looking at compositional analysis of the glass core and a visual analysis of the corrosion layers using secondary electron imaging at various magnifications.

4.Results

4.1 LED Digital Microscope

The results of the LED digital microscope surface investigation showed that many of the samples suffer from pitting corrosion. From visual analysis, it was hard to determine whether the darker spots were manganese browning or artificial dirt from burial conditions. The corrosion colours varied from white, yellow, to a pale blue powdery surface with some evidence of iridescence on all tesserae. As you can see from figure 28 below, this surface was typical for all tesserae observed under the digital microscope. Number 14 had little evidence of corrosion with a small film of iridescence on the tesserae as seen in figure 29 below. More detailed notes of observations, such as anomalies in corrosion patterns, are presented in the table 1 of the appendix. All images taken for this study can be seen in the appendix of this report.

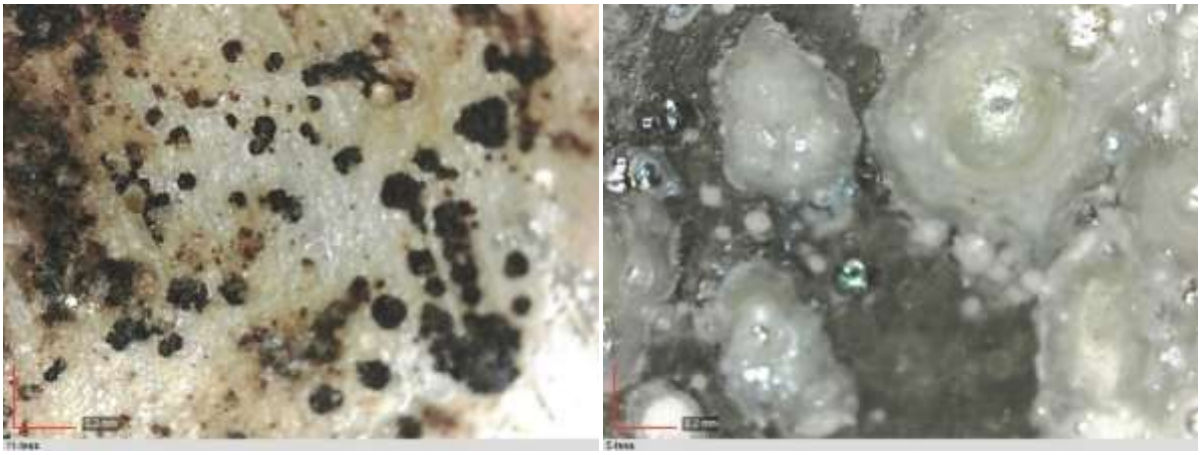

Figure 29: Number 11 tesserae on the left showing surface accretions or Mn browning. Number 5 tesserae on the right with pitting corrosion and iridescence.

Figure 30: Number 14 tesserae which exhibited little to no corrosion products except a thin film of iridescence.

4.2. Reflected Light Microscopy

Investigation into the corrosion layers and inclusions was done using Reflected Light Microscopy under various magnifications to detect any anomalies seen in the glass matrix or corrosion products. There are two tesserae which seem to be green under LED microscope however are a light green almost colourless in their matrix as seen in figure 30 below. Other interesting observations include the particles of copper and unidentifiable black inclusions, possibly iron particles, in the matrix of the glass as seen in figure 31 and 32 below. Based on the observations from the Reflected Light Microscopy, the browning on the surface of the tesserae is superficial from burial conditions. Samples 1, 3 and 10 which have a natural blue tint to the glass core exhibit corrosion that is less than 200 microns thick while the rest of the samples exhibit a high amount of corrosion over 500 microns in thickness. There are also distinctive hydration layers that are seen in the corrosion layers and later will be discussed when observing the line scans done with SEM. All images taken for this study can be seen in the appendix of this report.

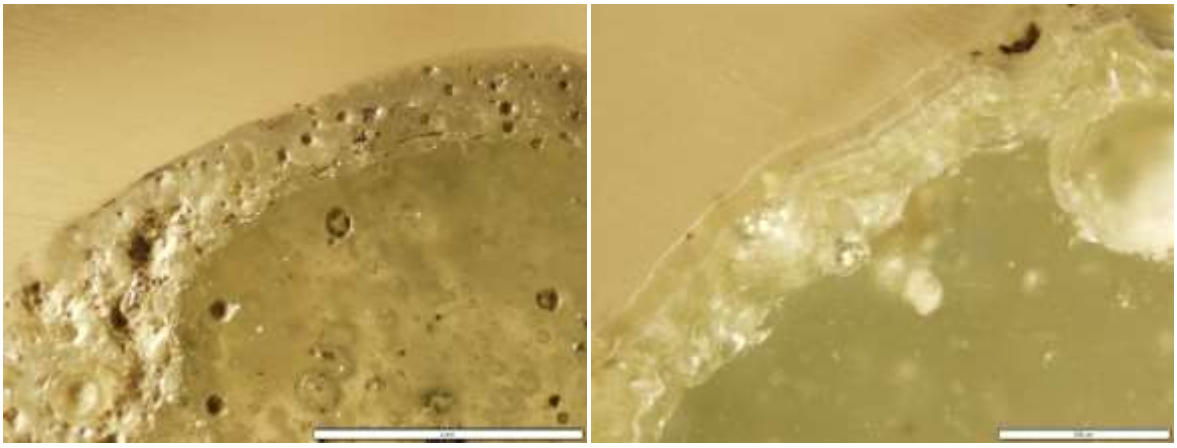

Figure 31: green tesserae-5 on the left and green tesserae-4 on the right seem like colorless glass under reflected light

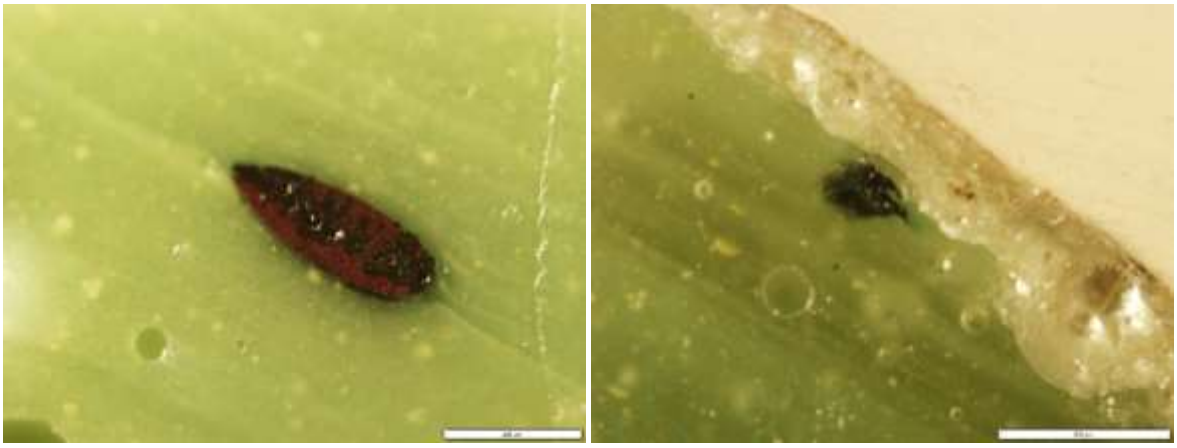

Figure 32: green tesserae-13 on the left showing red inclusion and green tesserae-2 on the right showing black inclusions, possible iron particles.

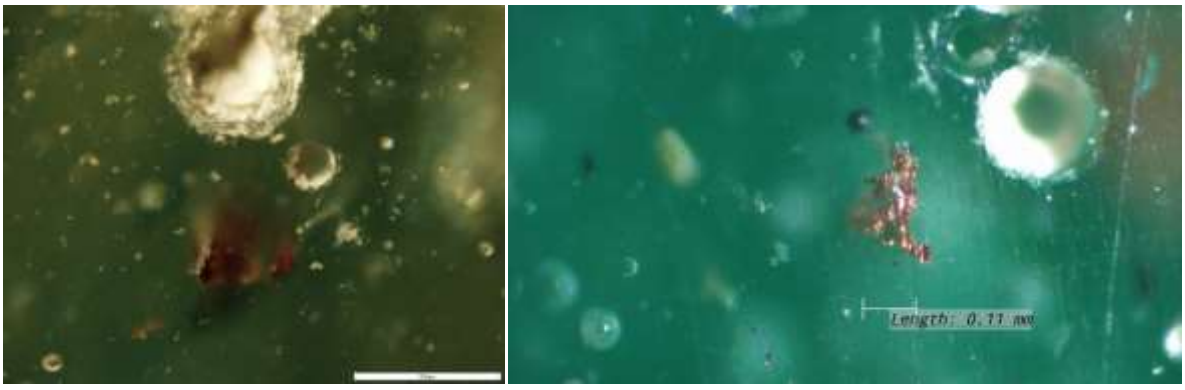

Figure 33: Blue tesserae-10 on the left and Blue tesserae-9 on the right showing copper inclusions

4.3 Portable X-ray Fluorescence

The calibration curve used for the analysis of glass cannot quantify elements with an atomic number above 30 and therefore lead and sulfur cannot be quantified to include in this data. Based on the results of the p-XRF data, there is a significant underestimation of sodium because standard Roman glass should have between 13-20 weight percent of sodium dioxide, which is soda used to create the glass. However, due to the burial conditions in which the

glass tesserae were found, there was a significant degree of alkali loss due to a leaching effect as described in the section titled 1.4 *Glass Corrosion* presented earlier in this thesis. There is also network dissolution and ion exchange between the outside environment and the glass which explains the higher amounts of potassium and magnesium seen in the p-XRF analysis. The underestimation is due to the corrosion left on the surface when p-XRF was carried out on the glass tesserae as the research question involved an investigation in the chemical analysis of the corrosion and core glass. The high calcium and sulfur content seen in sample 7 could be due to the residual mortar that was left within the pores of the tesserae as this one was especially difficult to surface clean prior to analysis.

Average XRF values (wt%) normalized to 100% based on four scans per sample											
sample	**colour**	**Na_2O**	**MgO**	**Al_2O_3**	**SiO2**	**P_2O_5**	**SO_3**	**K_2O**	**CaO**	**MnO**	**FeO**
1	blue	2.43	0.81	7.34	79.72	0.88	1.71	2.93	2.88	0.09	1.21
2	green	5.54	0.78	5.05	71.46	4.73	4.87	3.03	3.40	0.16	0.99
3	blue	5.62	1.51	6.66	74.08	1.08	3.17	2.08	4.60	0.23	0.96
4	green	7.15	0.44	5.60	78.07	0.53	1.02	3.43	2.70	0.13	0.93
5	green	4.73	0.65	4.85	79.81	0.40	2.18	3.66	2.30	0.07	1.35
6	green	5.85	1.16	6.07	71.46	1.91	6.75	2.07	3.34	0.08	1.32
7	blue	3.33	1.92	5.05	51.91	1.00	11.40	2.12	21.73	0.07	1.48
8	blue	4.61	0.52	5.90	78.88	0.36	1.98	3.20	3.24	0.18	1.12
9	blue	4.65	0.40	6.84	77.68	0.80	0.53	5.00	2.60	0.07	1.44
10	blue	7.94	0.78	5.88	76.94	0.73	1.04	2.05	3.55	0.17	0.92
11	green	5.78	1.60	5.41	69.70	5.05	5.03	2.91	3.37	0.11	1.05
12	green	5.13	1.30	5.84	69.66	3.40	8.20	2.37	2.61	0.05	1.43
13	green	0.92	1.34	7.04	62.39	7.48	10.49	4.08	5.10	0.09	1.06
14	blue	5.50	4.25	5.02	66.77	0.61	9.65	2.11	5.06	0.19	0.85

Statistics of the average values in pXRF										
	Na_2O	**MgO**	**Al2O3**	**SiO2**	**P_2O_5**	**SO_3**	**K_2O**	**CaO**	**MnO**	**FeO**
Mean	4.94	1.25	5.90	72.04	2.07	4.86	2.93	4.75	0.12	1.15
Median	5.32	0.99	5.86	72.77	0.94	4.02	2.92	3.36	0.10	1.09
Mode	0.92*a	0.78	5.05	71.46	0.36*a	0.53*a	2.05*a	2.30*a	0.07	0.85*a
Std. Deviation	1.80	0.98	0.81	7.85	2.22	3.81	0.89	4.97	0.06	0.22
Minimum	0.92	0.40	4.85	51.91	0.36	0.53	2.05	2.30	0.05	0.85
Maximum	7.94	4.25	7.34	79.81	7.48	11.40	5.00	21.73	0.23	1.48

The automatic quantification process attributes part of the iron Kα1 to manganese, especially in samples with certain iron and manganese ratios, thus underestimating the former and overestimating the latter. To correct this overlap, software is required to perform a deconvolution process for the spectrum, which is not available at this time. Below is a graph showing the K alpha of iron and the K beta of manganese which have overlapping spectrum bands.

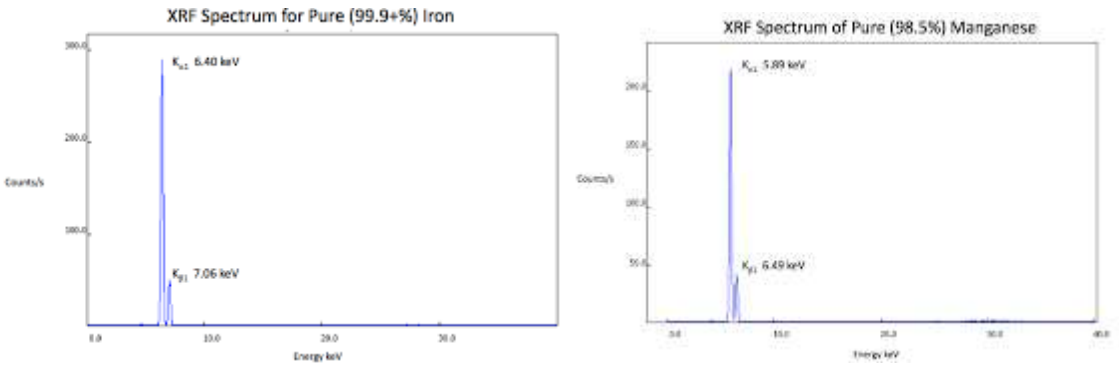

Figure 34: Spectrum for Iron and Manganese on XRF showing the Kα1 of iron has almost identical energy with the Kβ1 of manganese.

4.4. Scanning Electron Microscopy – Electron Dispersion Spectroscopy

Three scans were done on each sample to ensure there were enough statistical information to process the quantitative data. There was also a line scan done on each of the sample to better characterize the corrosion layers seen on the tesserae. Statistical data was processed by IBM SPSS Statistics software provided by Queen's University. Based on the average weight percent of oxides of each sample, the glass seems to be the typical soda lime silica type glass that is described in the previous chapters above based on the low concentrations of potassium oxide, magnesium oxide and phosphorus pentoxide, indicating the use of natron as a flux (Henderson, 2013). Below is a table of the average weight percentage of each oxide using SEM.

Average wt% of oxides in each sample using SEM, based on three scans per sample														
sample	**colour**	**Na_2O**	**MgO**	**Al_2O_3**	**SiO_2**	**P_2O_5**	**SO_3**	**K_2O**	**TiO_2**	**CaO**	**FeO**	**CuO**	**PbO**	**Cl**
1	Blue	15.31	0.5	1.96	69.43	0	0	0.74	0.28	5.57	0.49	1.31	3.24	1.17
2	Green	17.82	0.55	2.10	70.43	0	0.73	0.64	0	5.31	0.42	0.78	0	1.23
3	Blue	16.39	0.46	2.11	68.55	0	0	0.57	0	5.57	0.53	1.51	3.16	1.17
4	Green	17.33	0.57	2.01	71.15	0.32	0.43	0.65	0	5.54	0.42	0.51	0	1.19
5	Green	21.68	0.59	2.08	70.23	0	0	0.44	0	3.95	0	0	0	1.03
6	Green	16.45	0.61	1.83	68.05	0	0	0.63	0	5.24	0.54	0.97	4.48	1.20
7	Blue	16.09	0.51	1.89	72.43	0	0	0.68	0	5.63	0.54	1.00	0	1.24
8	Blue	16.14	0.48	1.9	71.91	0	0.6	0.66	0	5.45	0.40	1.22	0	1.24
9	Blue	18.43	0.49	1.95	70.81	0	0	0.70	0	4.59	0	1.89	0	1.13
10	Blue	15.54	0.48	1.98	72.49	0	0	0.66	0	6.02	0.33	1.29	0	1.21
11	Green	17.51	0.63	2.03	70.32	0.02	0.86	0.68	0	5.53	0.41	0.68	0	1.33
12	Green	18.03	0.54	2.09	65.83	0	0	0.62	0	4.41	0.41	0.9	6.14	1.02
13	Green	16.24	0.55	1.98	63.13	0	0	0.6	0	3.94	0.48	2.94	9.04	1.10
14	Blue	4.48	4.26	5.44	65.83	0	7.51	6.58	0.28	3.54	1.42	0	0	0.66

Statistics of the average values in SEM													
	Na_2O	MgO	Al_2O3	SiO_2	P_2O_5	SO_3	K_2O	TiO_2	CaO	FeO	CuO	PbO	Cl
Median	16.45	0.54	1.98	70.32		0	0.65		5.45	0.42	0.10	0	1.14
Mode	15.31*a	0.48	1.83*a	63.13*a		0	0.68		5.57	0*a	0*a	0	1.17*a
Minimum	15.31	0.46	1.83	63.13	0	0	0.44	0	3.94	0	0.00	0	0.66
Maximum	21.68	0.63	2.11	72.49	0.32	0.86	0.74	0.28	6.02	0.54	2.94	9.04	1.33
St. Dev.	1.67	0.05	0.09	2.69	0.09	0.33	0.73	0.08	0.68	0.18	0.71	2.99	0.08

Based on data above, glass tesserae #14 was an outlier due to surface analysis as it was not cut and prepared into a cross section. This sample exhibited little to no surface corrosion and was therefore not cut into a cross section due to the research question guiding the experimental. This data was removed for a better visual for the rest of the data in the following bi-plot charts. Figure 35 shows the weight concentrations of potassium and magnesia in the glass matrix of the tesserae. This shows that the main alkali source is natron due to the low amount of magnesia and potassium concentrations. A glass made with potash as the main alkali source would be in the upper right quadrant of the chart with weight concentrations of 2-10% for magnesia and 0-18% for potassium based on Artioli (2010) and Henderson (2013).

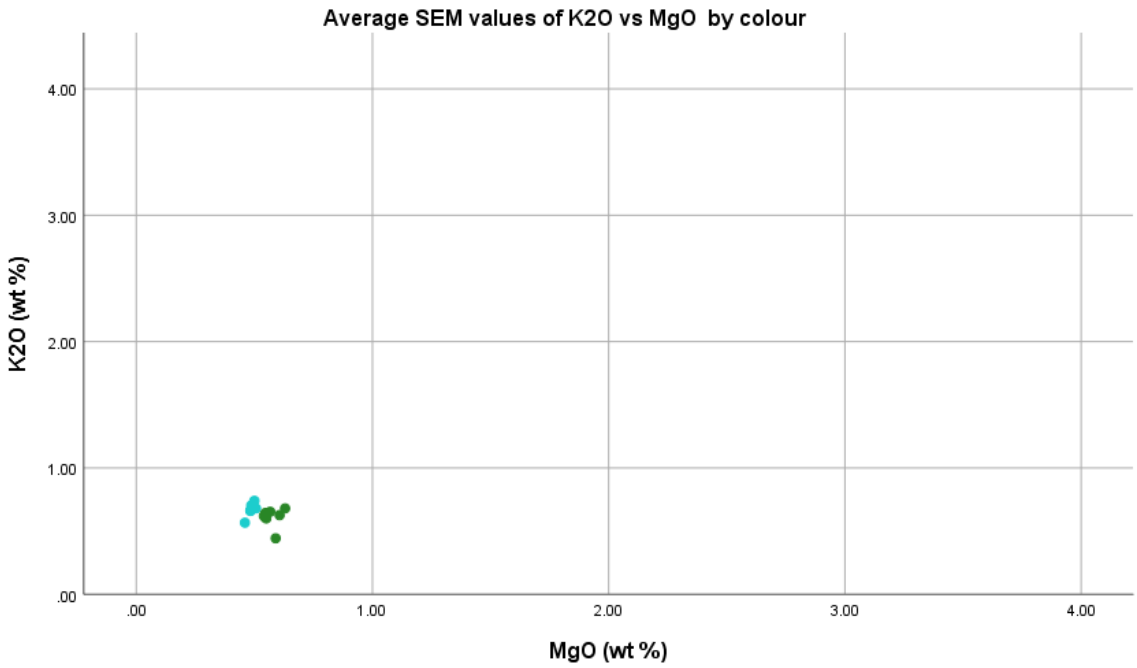

Figure 35: Potassium vs Magnesia concentrations based on average SEM values

Figure 36 below shows the weight concentrations of soda and alumina in the glass matrix of the tesserae based on average SEM values. This suggests that the sand used for the

creation of the glass tesserae came from a single source and could be a typical soda-lime-silica composition of glass based on the potassium and magnesia concentrations being 0-1 weight percent as mentioned in Artioli (2012) and Henderson (2013).

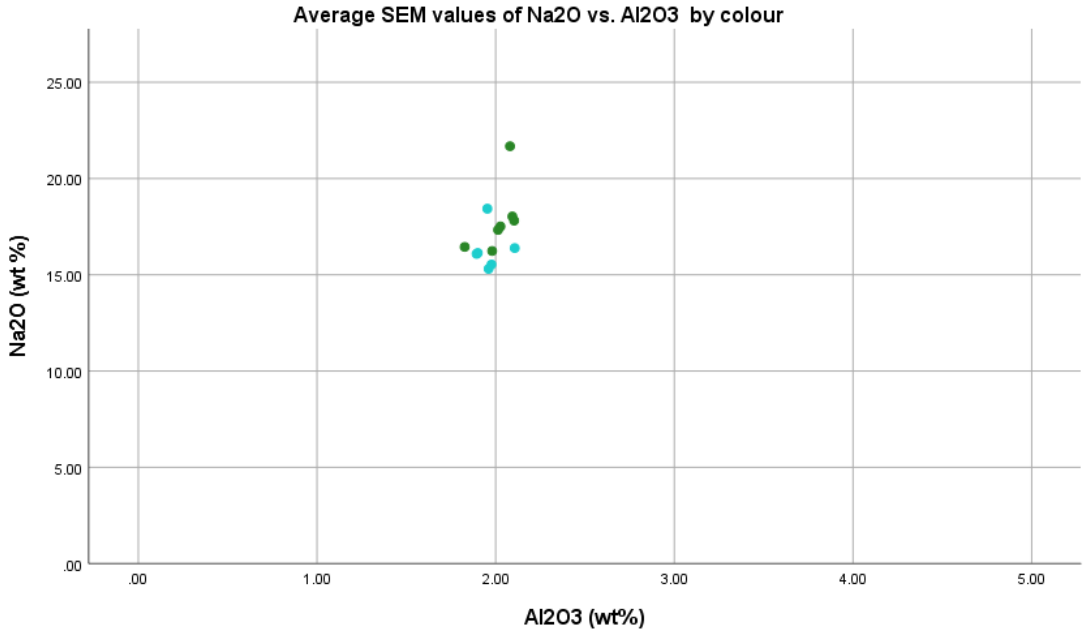

Figure 36: Soda vs alumina concentrations based on average SEM values.

Figure 37 shows iron against alumina weight concentrations in the glass matrix. This confirms the typical soda lime silica glass composition with levels of iron oxides between 0-1 weight percent and potassium levels between 0-1 weight percent as seen in the figure 35 based on Artioli (2012) and Henderson (2013). The iron concentrations of the tesserae suggest that the source of the silica used is from a singular area. This conclusion is based on the results found during the analysis and further corroborated by other observation made by Vataj et al., who analyzed glass tesserae from the 4th century CE from three different sites in Albania.

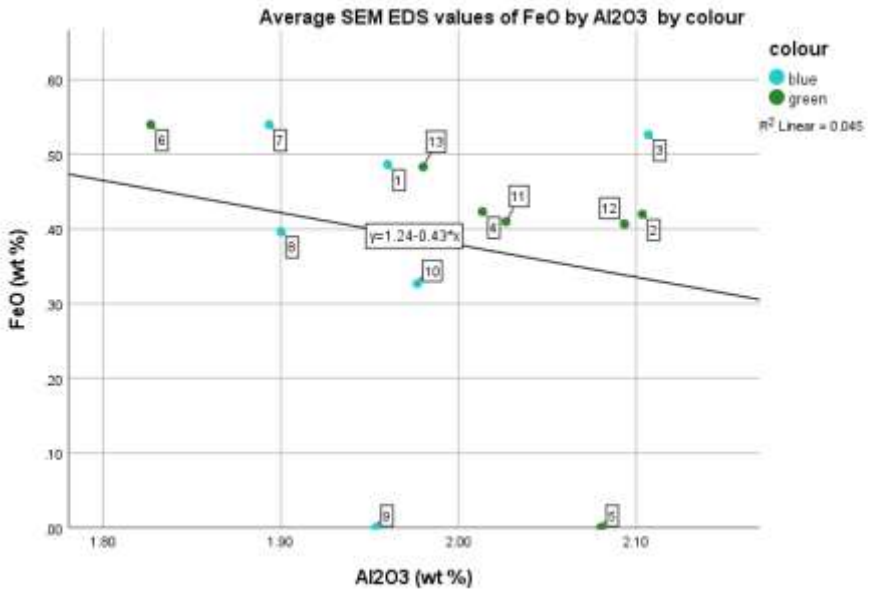

Figure 37: iron and alumina concentrations based on average SEM values

Results from the line scans done on the 13 samples along with the complimentary Reflected Light Microscopy show that there is no correlation between the core glass composition and the severity of the corrosion and surface alteration layer. The line scans revealed there was a depletion of silica and sodium (natron) as expected from the de-alkalization process that was presented earlier in section 1.4 *Glass corrosion* of this thesis. There was also significant drops noted in between layers, a phenomenon that occurs when there is significant changes in the moisture of the environment, such as heavy rainfall that changed the groundwater where these tesserae were buried, leading to a distinct layer of silica that was leached and later redeposited on the surface of glass to form this corrosion layer. Samples 1, 3, and 10 are less than 200 microns thick exhibiting a less drastic drop in silica levels in comparison to the samples which had corrosion layers over 200 microns in thickness, showing distinct layers of ion exchange.

Below is a table that shows the increase, decrease, and relative stability of all the observed elements when line scans were completed as well as the overall thickness of the corrosion layers seen on each tesserae. An increase in the amount seen would suggest an enrichment of the surface and ion exchange that was later redeposited on the surface of the tesserae. The decrease would suggest a depletion of the components from the glass and either re-deposited on the surface in the case of silica or to the surrounding environment. No change as labelled in the chart would suggest that the element was relatively stable and did not exhibit any depletion or enrichment, in other words there were not any up or downward trends observed on the graph.

Elemental and visual observations made during SEM line scans of the corrosion layers on the glass tesserae				
Sample number	Thickness of corrosion (µm)	Increase	Decrease	No Change
1	150	K, Al,	Ca, Na, Si	Mg
2	900	K, Al, Ca	Na, Si	Mg
3	150	K, Al,	Ca, Na, Si	Mg
4	300	K	Al, Ca, Na, Si	Mg
5	400	K, Al,	Ca, Na, Si	Mg
6	400	K, Al, Ca	Na, Si	Mg
7	300	K, Al,	Ca, Na, Si	Mg
8	250	K, Al,	Ca, Na, Si	Mg
9	1000	K, Al,	Ca, Na, Si	Mg
10	100	K, Al,	Ca, Na, Si	Mg
11	200	K, Al,	Na, Si	Ca, Mg
12	200	K, Al,	Ca, Na, Si	Mg
13	600	K, Al, Ca	Na, Si	Mg

Through visual observations there seems to be some correlation between porosity of the tesserae and the severity of the corrosion which makes sense due to the corrosion phenomenon that was discussed earlier in this thesis in section 1.4 *Glass Corrosion.* The porous glass core is a physical manifestation of the ion exchange, or de-alkalization, that occurs between the core glass and the burial environment. This can be seen in the comparison between compact glass tesserae such as number 1 as seen in figure 38 and the more gaseous glass tesserae such as number 9 as seen in figure 39 below.

Figure 38: Glass tesserae #1 line scan showing the two significant surface alteration layers with the depletion of silicon as seen in the yellow line. The polarized light microscope image shows the surface alteration layers are no larger than 200 microns

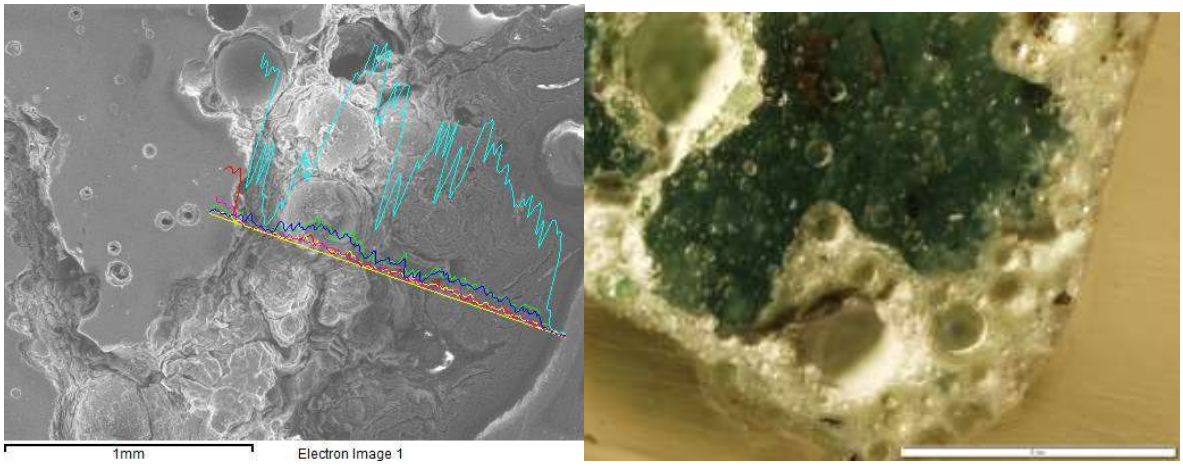

Figure 39: Glass tesserae #9 line scan showing three layers or more surface alteration layers with the depletion of silicon animated by the blue line on the SEM image. The polarized light microscope image shows the porosity of the glass tesserae as well as the severity of the corrosion larger than 200 microns.

Line scans were done on all the surface alteration layers of the glass tesserae and all showed varying levels of silicon depletion. As seen in the Reflected Light Microscopy and confirmed in the backscattered electron image, there are multiple layers of silica (silicon), soda (sodium), and lime (calcium) depletion seen in all the glass tesserae as seen in figure 40.

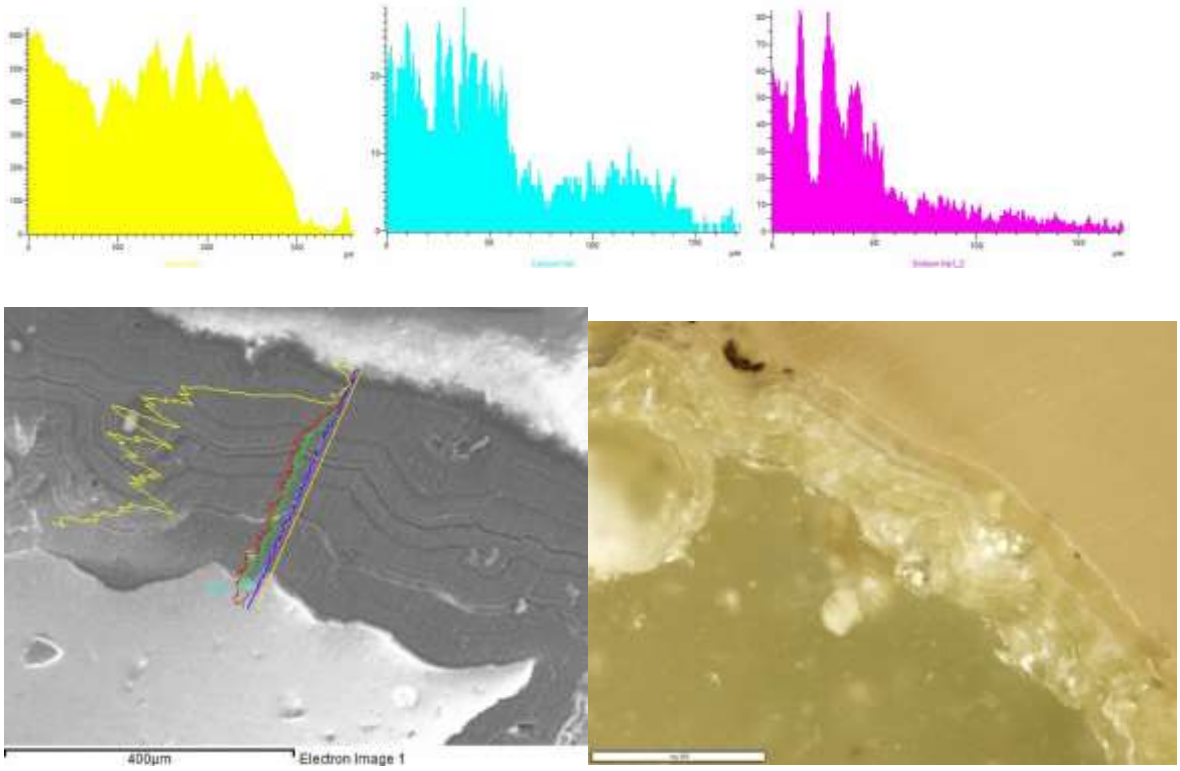

Figure 40: Above: Line scan of glass tesserae #4 corrosion layers, yellow= silicon, blue = calcium, purple = sodium. Bottom left: Line Scan of glass tesserae #4 (400 Microns) and Bottom right: PLM image under reflected light (500 microns)

Conclusion

The glass tesserae found near the Temple of Isis complex at the archaeological site of Stobi and subsequently studied in this thesis seem to be made from a typical soda lime silica recipe as described in previous sections. Through visual and chemical analysis there is a further understanding of the colour of the tesserae created by the natural impurities of the source material, such as copper and iron, used in creating the glass. This can be seen in Reflected Light Microscopy and confirmed with Scanning Electron Microscope analysis which is exemplified in samples 1, 2, 3, 6, 7, 8, 9, 10, and 13 where there are visible copper and iron impurities observed. The porosity of the core glass seems to affect the severity of the corrosion as seen in the Reflected Light Microscopy and Scanning Electron Microscopy due to the increased surface area of the interstices of the pores which allow for increased chances of hydration, therefore increasing the amount of corrosion seen on the surface in a cycle of de-alkalization that could have been occurring since removed from their stable burial environment. This can be seen in samples 4, 5, 6, 7, 8, 9, 10 and 11 where the thickness of the corrosion layers exceeds 200 microns. It is unclear if the porosity is due to the degradation mechanism at work during burial or if this was a manufacturing flaw when the glass was produced at a primary workshop and later re-worked at a secondary workshop. It begs the question to understand if glass is more susceptible to corrosion at faster rates due to the additional impurities such as the materials involved in re-heating and re-working the glass at a secondary workshop during the Roman period.

In conclusion, the research question proposed had garnered more questions after the initial analysis and results were obtained. The proposed question was to find some correlation between the corrosion patterns observed and the composition of the glass tesserae. Once the composition of the glass was confirmed, questions around the storage conditions after they were excavated and the conditions in which they were found, are contributing factors that affected the corrosion patterns observed on the glass tesserae. The burial environment and storage conditions, which can further degradation due to moisture exposure are uncontrolled variables that could not be monitored in this thesis to see how they fluctuate and affect the corrosion rate and amount of degradation seen on the glass tesserae. There is also the question regarding primary versus secondary workshops and the effect that re-working glass material has on the composition of the glass, and the subsequent degradation of that glass, based on whether it is primary or secondary material.

Future Work

The present thesis has allowed for a further understanding of the corrosion mechanisms that are involved in the degradation of glass tesserae through microscope analysis of the glass components and an investigation into the layers that result from de-alkalization and re-hydration of the glass. Through observations of the corrosion patterns seen on the glass tesserae in utilizing SEM and PLM analysis, there is a visual example of how the chemical interactions that take place during burial conditions affect the surface of the tesserae. Further work includes an investigation into the various conditions that cause the complete powdering and disintegration of glass and stone as seen in the figure mentioned in the conservation issues section of this thesis. A survey of corrosion patterns and chemical composition of the glass material found at the archaeological site of Stobi, North Macedonia would be useful to see if it this degradation phenomenon is related to the conditions in which they were found, the composition of the material and whether it was primary or secondary sourced material, or the subsequent treatment and storage conditions that is leading to the disintegration of the glass tesserae.

This is not an isolated incident as many other fragments, both wall and floor mosaics, that contain glass tesserae face similar deterioration patterns of lamination, powdering, and completed disintegration, some of which are stored in a controlled museum environment. An example of this is seen in the mosaics preserved at the archaeological museum of Thessaloniki, Greece which have excellent examples of floor and wall mosaic fragments yet are at risk for completed disintegration.

Figure 41: Floor mosaic fragments at the archaeological museum of Thessaloniki showing powdering and corrosion on the green and blue tesserae. Photos taken by Paige Van Tassel.

Appendix

Table 1: Corrosion observations

Table of Corrosion observations					
Sample	**Weight**	**Colour of stable glass**	**LED digital microscope**	**Reflected Light Microscopy**	**SEM – SEI line scan**
1	1.88g	blue	Brown and white corrosion products present on the surface. Abrasion and surface pitting.	Total amount of corrosion layers smaller than 200 microns thick. Browning does not cross layers, only superficial.	Depletion of silicon and sodium within the corrosion layers, increase in alumina over 150 microns
2	1.42g	green	White and yellow corrosion products. Brown encrustations may be due to burial context and some evidence Mn browning. Abrasion on the surface of the tesserae under the microscope suggest that Mn browning is present.	Total amount of corrosion layers no larger than 500 microns thick with visible hydration layers. Browning only superficial.	Depletion of alumina and silica within the corrosion layers over 500 microns
3	0.99g	blue	Surface corrosion is white and yellow powdery surface. There is surface pitting and abrasion from burial context.	Total amount of corrosion layers larger than 200 microns thick.	Gradual depletion of silica and alumina over 200 microns with one drastic drop in silica indicating the gel layer.
4	0.50g	green	Surface corrosion is whitish and iridescent. Small evidence of Mn browning present. Abrasion and pitting present on the surface of the tesserae.	Total amount of corrosion layers no larger than 500 microns thick. Visible hydration layers. Browning only superficial. Glass matrix seems colourless under reflected light.	Corrosion layers show depletion of silica and alumina with a noticeable drop between gel layers.
5	0.69g	green	The corrosion is whitish to light blue in colour which is powdery. Surface pitting of the corrosion layers.	Total amount of corrosion layers larger than 500 microns thick with high amount of bubbling within corrosion layers. Glass matrix seems colourless	Corrosion layers show a depletion of silica and alumina over 400 microns. There are two different phases of corrosion layers

				under reflected light.	
6	0.82g	green	The surface of the corrosion layers is whitish yellow with some evidence of Mn browning. Some evidence of iridescence on the surface of the tesserae.	Total amount of corrosion layers no larger than 500 microns thick. Browning only superficial.	Corrosion layers show depletion of silica and alumina with drastic changes between gel layers.
7	0.75g	blue	The surface corrosion is powdery in whitish blue in colour.	The total amount of corrosion layers is no lager than 500 microns thick with visible hydration layers. Copper streaks and copper inclusions	Corrosion layers show a depletion of silica and alumina with drastic changes between gel layers.
8	1.40g	blue	The surface corrosion is whitish blue and powdery. There is pitting and abrasion from burial context.	Total amount of corrosion layers is larger than 500 microns thick in some areas with visible hydration layers. Light blue under reflected light.	Corrosion layers show a depletion of silica and alumina
9	0.38g	blue	Whitish blue powdery corrosion products with some evidence of pitting corrosion and iridescence.	Total amount of corrosion layers larger than 500 microns thick. High amount of copper inclusions found throughout the glass matrix.	Large number of voids in the corrosion layers, making it a large line scan showing gradual depletion of alumina and silica
10	1.14g	blue	Visible delamination of the corrosion layers. There is a lower amount of powdering corrosion product. Pitting corrosion and iridescence are present.	Total amount of corrosion layers no larger than 200 microns thick with a visible hydration layer. Large copper inclusions found in the glass matrix.	Small area of around 100 microns showing a gradual depletion of alumina and silica.
11	0.30g	green	Surface is whitish blue powder, with some evidence of pitting corrosion, Mn-browning, and iridescence.	Total amount of corrosion layers no larger than 500 microns thick with visible hydration layers. Browning only superficial	Corrosion layer shows a sudden drop in alumina and silica around 30 microns into the sample. No drastic changes in hydration layers.

12	0.95g	green	Yellowish green powdery surface with some evidence of Mn browning, pitting corrosion and iridescence. Visible delamination of the corrosion layers.	Total amount of corrosion layers no larger than 500 microns thick with visible hydration layers. Browning only superficial.	Gradual depletion of silica and alumina over 200 microns with one sudden drop in silica indicating a gel layer.
13	0.90g	green	Yellowish green powdery surface with some evidence of pitting corrosion and iridescence.	Total amount of corrosion layers larger than 500 microns with visible hydration layers. Black and red inclusions found in the glass matrix.	Significant change in alumina and silica concentrations with a change in hydration layer. Two different sections of corrosion, one darker and 100 microns, the other 500 microns.
14	1.02g	blue	Thin film of iridescence otherwise, little to no corrosion products present on the glass surface.	NA (cross section not done on sample)	Small surface pitting. Spot analysis shows higher amounts of SO3 and K2O compared to cross section analysis of other samples.

Table 2: pXRF analytical data

pXRF values (wt%) normalized to 100%													
sample	**spectrum**	**colour**	**Na_2O**	**MgO**	**Al_2O_3**	**SiO_2**	**P_2O_5**	**SO_3**	**K_2O**	**CaO**	**MnO**	**FeO**	**SUM**
1	1	blue	2.39	0.70	7.87	80.68	0.51	1.04	3.37	2.24	0.07	1.12	100
1	2	blue	2.47	0.75	7.41	80.23	0.58	1.06	3.30	2.86	0.08	1.27	100
1	3	blue	1.66	0.71	8.20	80.33	0.70	1.21	3.52	2.42	0.08	1.15	100
1	4	blue	2.13	1.11	7.53	76.32	2.54	2.84	3.04	2.78	0.08	1.62	100
1	5	blue	2.84	0.90	5.59	80.17	0.53	3.14	1.28	4.52	0.13	0.90	100
1	6	blue	3.10	0.69	7.45	80.57	0.43	0.96	3.06	2.48	0.08	1.20	100
2	1	green	5.46	0.32	5.10	77.28	1.02	3.27	2.82	3.52	0.10	1.10	100
2	2	green	7.57	0.24	4.62	76.51	0.60	3.15	2.40	3.75	0.10	1.06	100
2	3	green	7.46	0.37	4.46	76.34	0.76	3.47	2.21	3.86	0.10	0.96	100
2	4	green	1.64	2.18	6.01	55.71	16.54	9.59	4.67	2.44	0.34	0.87	100
3	1	blue	2.34	1.85	8.72	75.83	1.49	2.46	3.78	1.91	0.06	1.55	100
3	2	blue	5.62	1.29	7.03	76.17	1.19	3.23	1.80	2.41	0.06	1.21	100
3	3	blue	7.15	1.25	5.00	69.84	0.30	3.25	1.33	11.13	0.74	nd	100
3	4	blue	7.37	1.67	5.87	74.49	1.35	3.73	1.41	2.94	0.06	1.10	100
4	1	green	9.08	0.08	4.26	78.21	0.38	0.84	2.69	3.44	0.11	0.91	100
4	2	green	8.10	0.44	4.36	78.61	0.39	0.97	2.68	3.42	0.11	0.91	100
4	3	green	7.15	0.20	4.76	79.38	0.47	1.15	2.76	3.10	0.10	0.95	100
4	4	green	4.30	1.05	9.01	76.09	0.90	1.11	5.59	0.82	0.18	0.95	100
5	1	green	4.85	0.59	4.82	80.08	0.48	2.07	3.35	2.50	0.08	1.17	100
5	2	green	8.45	0.51	4.42	77.59	0.41	1.93	3.16	2.35	0.07	1.12	100
5	3	green	3.33	0.38	4.61	82.23	0.20	1.40	3.89	2.27	0.07	1.62	100
5	4	green	2.28	1.13	5.55	79.36	0.51	3.30	4.23	2.09	0.07	1.48	100
6	1	green	4.93	1.02	4.88	73.15	1.89	7.64	1.85	3.22	0.06	1.36	100

6	2	green	6.97	0.78	5.56	73.59	1.08	6.37	1.65	2.64	0.05	1.32	100
6	3	green	8.77	1.30	4.79	68.00	1.69	7.28	1.24	5.77	0.18	0.98	100
6	4	green	2.71	1.53	9.03	71.09	2.97	5.73	3.55	1.75	0.04	1.60	100
7	1	blue	3.02	0.08	5.33	82.60	0.32	0.66	3.50	3.16	0.10	1.25	100
7	2	blue	3.71	0.40	5.46	81.57	0.36	0.75	3.82	2.56	0.10	1.26	100
7	3	blue	3.35	3.37	3.30	15.67	1.67	25.23	0.37	45.65	0.03	1.35	100
7	4	blue	3.23	3.84	6.12	27.80	1.63	18.95	0.78	35.55	0.04	2.07	100
8	1	blue	6.68	0.23	4.54	79.61	0.32	1.46	2.12	3.89	0.12	1.03	100
8	2	blue	4.62	0.72	5.69	79.28	0.45	2.04	3.09	2.92	0.14	1.03	100
8	3	blue	5.95	-.22	4.63	80.21	0.29	1.46	2.25	4.21	0.14	1.09	100
8	4	blue	1.22	1.34	8.73	76.44	0.39	2.97	5.34	1.93	0.32	1.34	100
9	1	blue	6.18	0.25	5.94	78.08	0.46	0.65	4.02	3.05	0.07	1.30	100
9	2	blue	5.97	0.40	5.75	78.30	0.46	0.61	4.00	3.14	0.08	1.29	100
9	3	blue	1.79	0.56	8.83	76.66	1.47	0.32	6.98	1.61	0.05	1.72	100
9	4	blue	4.45	0.45	6.05	79.77	0.47	0.59	4.16	2.68	0.07	1.31	100
10	1	blue	7.37	0.29	4.77	79.19	0.52	0.82	1.58	4.41	0.14	0.91	100
10	2	blue	9.64	0.36	4.66	77.19	0.59	0.98	1.53	4.12	0.18	0.75	100
10	3	blue	11.13	1.30	5.95	73.66	0.93	1.39	1.57	2.99	0.08	0.99	100
10	4	blue	3.60	1.16	8.13	77.73	0.87	0.97	3.53	2.69	0.28	1.02	100
11	1	green	6.35	1.10	5.13	75.72	1.22	3.37	2.43	3.55	0.09	1.03	100
11	2	green	3.75	1.08	5.73	76.02	2.10	3.90	3.02	3.21	0.10	1.09	100
11	3	green	2.07	2.62	5.75	56.07	15.51	9.44	4.00	3.26	0.18	1.11	100
11	4	green	10.96	1.59	5.02	70.98	1.35	3.43	2.19	3.44	0.09	0.96	100
12	1	green	7.88	0.64	4.86	73.91	0.77	5.73	1.86	3.10	0.06	1.19	100
12	2	green	4.36	1.69	5.44	65.67	6.25	10.30	2.26	2.45	0.04	1.52	100
12	3	green	5.14	1.03	5.34	74.88	0.96	6.15	2.13	3.01	0.06	1.29	100
12	4	green	3.13	1.84	7.73	64.19	5.63	10.62	3.24	1.87	0.04	1.72	100
13	1	green	1.87	1.55	8.06	67.42	3.89	8.69	4.25	2.94	0.03	1.29	100
13	2	green	nd	1.52	3.66	47.64	17.40	14.95	2.35	12.23	0.26	nd	100
13	3	green	1.10	1.13	8.12	67.30	4.21	9.15	4.98	2.49	0.03	1.50	100
13	4	green	0.70	1.17	8.34	67.20	4.43	9.15	4.76	2.74	0.03	1.47	100
14	1	blue	5.61	3.98	5.00	67.82	0.53	8.53	2.05	5.42	0.22	0.84	100
14	2	blue	7.06	4.42	4.87	65.91	0.58	10.04	1.83	4.37	0.15	0.78	100
14	3	blue	3.82	4.36	5.19	66.58	0.71	10.37	2.46	5.38	0.21	0.91	100

Statistics of the values in pXRF										
	Na_2O	**MgO**	**Al_2O_3**	**SiO2**	**P_2O_5**	**SO_3**	**K_2O**	**CaO**	**MnO**	**FeO**
Mean	4.84	1.18	5.95	72.44	2.05	4.66	2.93	4.68	0.12	1.16
Median	4.45	1.03	5.55	76.32	0.76	3.15	2.82	3.01	0.08	1.12
Mode	7.15*a	0.08*a	5.00*a	15.67*a	0.32*a	0.97*a	4.00	2.94*a	0.08*a	0.91
Std. Deviation	2.68	1.05	1.52	12.03	3.68	4.90	1.28	7.22	0.11	0.35
Minimum	0.00	-.22	3.30	15.67	0.20	0.32	0.37	0.82	0.03	0.00
Maximum	11.13	4.42	9.03	82.60	17.40	25.23	6.98	45.65	0.74	2.07

*a - Multiple modes exist. The smallest value is shown

Standard Deviation of pXRF values based on three scans per sample											
sample	**colour**	**Na_2O**	**MgO**	**Al_2O_3**	**SiO_2**	**P_2O_5**	**SO_3**	**K_2O**	**CaO**	**MnO**	**FeO**
1	blue	0.51	0.17	0.91	1.68	0.82	1.00	0.83	0.84	0.02	0.24
2	green	2.77	0.94	0.70	10.51	7.88	3.15	1.13	0.65	0.12	0.10
3	blue	2.32	0.29	1.61	2.92	0.54	0.52	1.15	4.37	0.34	0.67
4	green	2.06	0.43	2.28	1.41	0.25	0.14	1.44	1.26	0.04	0.02
5	green	2.70	0.33	0.50	1.92	0.14	0.80	0.49	0.17	0.00	0.24
6	green	2.61	0.32	2.00	2.55	0.79	0.87	1.02	1.73	0.07	0.25

7	blue	0.29	1.96	1.22	35.20	0.76	12.61	1.79	22.18	0.04	0.39
8	blue	2.42	0.67	1.96	1.68	0.07	0.71	1.49	1.03	0.09	0.15
9	blue	2.03	0.13	1.46	1.27	0.50	0.15	1.46	0.70	0.01	0.21
10	blue	3.27	0.53	1.61	2.34	0.20	0.24	0.99	0.84	0.08	0.12
11	green	3.87	0.72	0.39	9.37	6.99	2.95	0.80	0.16	0.04	0.07
12	green	2.01	0.56	1.28	5.51	2.94	2.62	0.60	0.57	0.01	0.24
13	green	0.78	0.22	2.26	9.83	6.61	2.99	1.20	4.76	0.11	0.72
14	blue	1.62	0.24	0.16	0.97	0.09	0.99	0.32	0.60	0.04	0.06

Table 3: SEM analytical data

Standard Deviation of oxides based on three scans per sample using SEM														
sample	**colour**	**Na_2O**	**MgO**	**Al_2O_3**	**SiO_2**	**P_2O_5**	**SO_3**	**K_2O**	**TiO_2**	**CaO**	**Fe2O3**	**CuO**	**PbO**	**Cl**
1	Blue	0.74	0.07	0.13	0.65	0	0	0.04	0.07	0.10	0.14	0.27	0.52	0.02
2	Green	0.20	0.04	0.08	0.16	0	0.18	0.06	0	0.08	0.04	0.10	0	0.07
3	Blue	0.18	0.02	0.25	0.25	0	0	0.01	0	0.12	0.21	0.25	0.49	0.06
4	Green	0.14	0.21	0.11	0.54	0.18	0.09	0.06	0	0.28	0.16	0.11	0	0.07
5	Green	0.13	0.26	0.15	0.50	0	0	0.01	0	0.14	0	0	0	0.06
6	Green	0.03	0.03	0.04	1.05	0	0	0.07	0	0.16	0.10	0.28	0.67	0.05
7	Blue	0.40	0.05	0.04	0.31	0	0	0.07	0	0.10	0.13	0.31	0	0.02
8	Blue	0.50	0.09	0.10	0.35	0	0.05	0.11	0	0.06	0.05	0.11	0	0.03
9	Blue	0.27	0.09	0.08	0.26	0	0	0.09	0	0.06	0	0.21	0	0.08
10	Blue	0.34	0.08	0.05	0.23	0	0	0.07	0	0.05	0.16	0.12	0	0.08
11	Green	0.30	0.07	0.14	0.58	0.03	0.22	0.11	0	0.09	0.12	0.26	0	0.09
12	Green	0.28	0.03	0.10	1.07	0	0	0.05	0	0.10	0.07	0.23	0.76	0.03
13	Green	0.29	0.01	0.14	0.99	0	0	0.04	0	0.18	0.13	1.30	0.27	0.12
14	Blue	1.77	0.50	0.40	7.24	0	5.47	2.61	0.25	0.84	0.20	0	0	0.21

Data of SEM results, normalized to 100%														
sample	**colour**	**spectrum**	**Na_2O**	**MgO**	**Al_2O_3**	**SiO_2**	**P_2O_5**	**SO_3**	**K_2O**	**TiO_2**	**CaO**	**FeO**	**CuO**	**PbO**	**Cl**
1	Blue	1	14.52	0.56	2.02	69.36	-	-	0.74	0.33	5.64	0.51	1.50	3.66	1.15
1	Blue	2	15.40	0.52	1.81	70.11	-	-	0.78	0.32	5.62	0.61	1.01	2.66	1.17
1	Blue	3	16.00	0.42	2.05	68.81	-	-	0.70	0.20	5.45	0.34	1.43	3.41	1.19
2	Green	1	17.64	0.58	2.12	70.43	-	0.70	0.67	-	5.40	0.39	0.76	-	1.31
2	Green	2	17.77	0.50	2.17	70.27	-	0.92	0.57	-	5.25	0.47	0.89	-	1.19
2	Green	3	18.04	0.56	2.02	70.58	-	0.56	0.69	-	5.27	0.40	0.69	-	1.19
3	Blue	1	16.31	0.46	2.39	68.83	-	-	0.56	-	5.67	0.77	1.25	2.6	1.17
3	Blue	2	16.59	0.44	1.94	68.35	-	-	0.57	-	5.44	0.44	1.54	3.47	1.23
3	Blue	3	16.26	0.48	1.99	68.47	-	-	0.57	-	5.6	0.37	1.74	3.41	1.11

4	Green	1	17.47	0.37	1.91	71.55	0.19	0.47	0.60	-	5.36	0.46	0.47	-	1.17
4	Green	2	17.33	0.54	2.00	71.36	-	0.49	0.64	-	5.39	0.56	0.43	-	1.26
4	Green	3	17.20	0.79	2.13	70.53	0.44	0.32	0.72	-	5.86	0.25	0.64	-	1.13
5	Green	1	21.64	0.89	2.25	69.74	-	-	0.45	-	4.06	-	-	-	0.96
5	Green	2	21.57	0.44	1.98	70.73	-	-	0.43	-	3.79	-	-	-	1.05
5	Green	3	21.82	0.44	2.01	70.21	-	-	0.45	-	4.00	-	-	-	1.07
6	Green	1	16.48	0.60	1.79	68.08	-	-	0.62	-	5.29	0.62	0.82	4.54	1.16
6	Green	2	16.44	0.64	1.82	66.99	-	-	0.70	-	5.37	0.43	1.30	5.12	1.19
6	Green	3	16.42	0.58	1.87	69.09	-	-	0.56	-	5.06	0.57	0.8	3.79	1.26
7	Blue	1	15.79	0.47	1.94	72.79	-	-	0.76	-	5.69	0.62	0.71	-	1.24
7	Blue	2	16.54	0.56	1.87	72.27	-	-	0.65	-	5.51	0.39	0.96	-	1.26
7	Blue	3	15.93	0.49	1.87	72.24	-	-	0.63	-	5.68	0.61	1.32	-	1.23
8	Blue	1	15.56	0.59	1.85	72.14	-	0.56	0.78	-	5.49	0.45	1.33	-	1.26
8	Blue	2	16.48	0.44	2.01	71.51	-	0.65	0.64	-	5.47	0.37	1.22	-	1.21
8	Blue	3	16.37	0.42	1.84	72.09	-	0.59	0.57	-	5.38	0.37	1.12	-	1.25
9	Blue	1	18.71	0.41	1.89	70.56	-	-	0.71	-	4.58	-	2.10	-	1.05
9	Blue	2	18.41	0.47	2.04	70.80	-	-	0.61	-	4.65	-	1.89	-	1.13
9	Blue	3	18.18	0.58	1.93	71.08	-	-	0.79	-	4.53	-	1.69	-	1.21
10	Blue	1	15.76	0.57	2.02	72.23	-	-	0.62	-	6.02	0.33	1.31	-	1.14
10	Blue	2	15.70	0.41	1.98	72.68	-	-	0.62	-	6.06	0.17	1.17	-	1.20
10	Blue	3	15.15	0.47	1.93	72.56	-	-	0.74	-	5.97	0.48	1.4	-	1.29
11	Green	1	17.16	0.55	2.04	70.98	0.06	0.61	0.79	-	5.51	0.50	0.40	-	1.40
11	Green	2	17.66	0.67	1.88	70.10	-	0.94	0.57	-	5.63	0.28	0.91	-	1.36
11	Green	3	17.71	0.67	2.16	69.89	-	1.03	0.68	-	5.45	0.45	0.73	-	1.23
12	Green	1	18.05	0.51	2.18	65.93	-	-	0.61	-	4.43	0.43	0.65	6.22	0.99
12	Green	2	18.30	0.57	2.11	64.72	-	-	0.67	-	4.3	0.33	1.10	6.85	1.03
12	Green	3	17.74	0.54	1.99	66.85	-	-	0.58	-	4.49	0.46	0.95	5.34	1.05
13	Green	1	16.44	0.54	1.83	62.08	-	-	0.55	-	3.76	0.54	4.44	8.73	1.10
13	Green	2	16.37	0.55	2.00	63.25	-	-	0.63	-	4.11	0.58	2.26	9.24	0.99

13	Green	3	15.9	0.56	2.11	64.05	-	-	0.62	-	3.94	0.33	2.13	9.14	1.22
14	Blue	1	6.02	3.79	5.42	69.53	-	4.59	4.98	0.13	3.17	1.50	-	-	0.86
14	Blue	2	4.88	4.20	5.85	70.47	-	4.11	5.16	0.13	2.95	1.57	-	-	0.68
14	Blue	3	2.55	4.78	5.05	57.48	-	13.82	9.59	0.57	4.5	1.19	-	-	0.45

Statistics of the wt % values run by SEM											
	Na_2O	MgO	Al_2O3	SiO_2	SO_3	K_2O	CaO	Fe_2O_3	CuO	PbO	Cl2
Mean	17.15	0.53	1.99	69.60	0.20	0.64	5.13	0.38	1.16	2.00	1.14
Median	16.54	0.54	1.99	70.27	0.00	0.63	5.39	0.43	1.10	0.00	1.18
Mode	16.37*a	0.44*a	1.87*a	62.08*a	0.00	0.57	5.45*a	0.00	0.00	0.00	1.19*a
St.Dev.	1.65	0.10	0.13	2.67	0.33	0.09	0.67	0.20	0.76	2.93	0.17
Minimum	14.52	0.37	1.79	62.08	0.00	0.43	3.76	0.00	0.00	0.00	0.45
Maximum	21.82	0.89	2.39	72.79	1.03	0.79	6.06	0.77	4.44	9.24	1.40

*a Multiple modes exist. The smallest value is shown

Images of LED, PLM, and SEM by tesserae

Tesserae 1

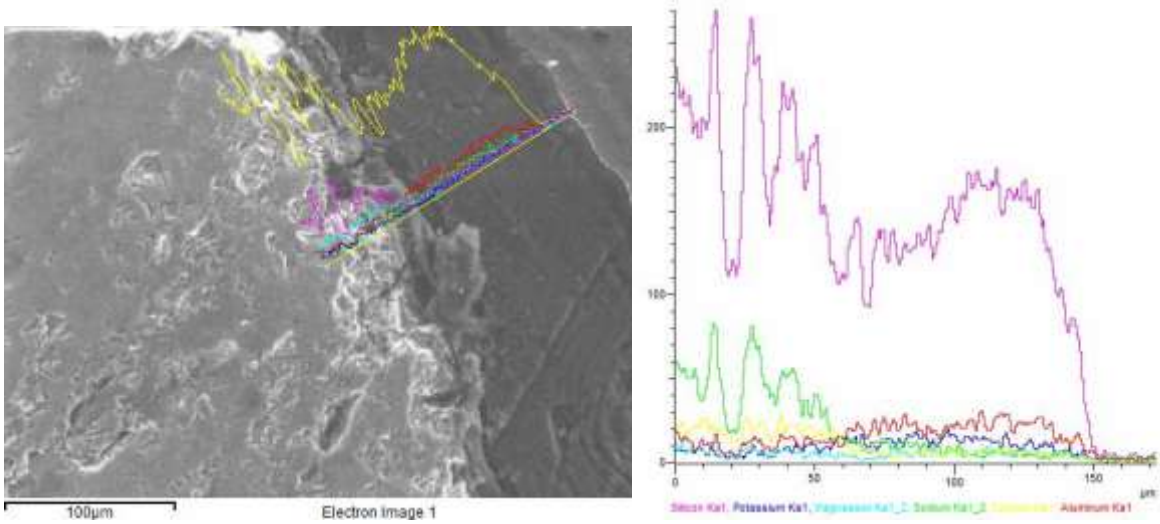

Tesserae 2

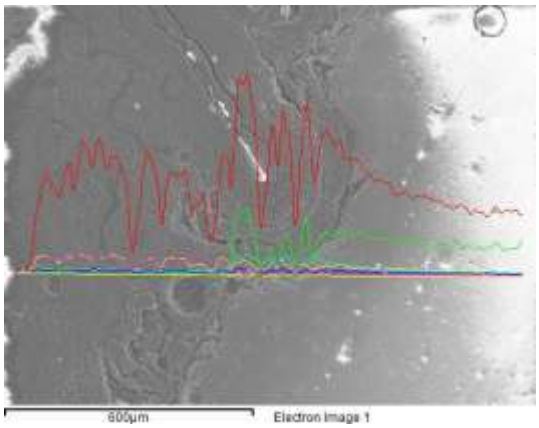

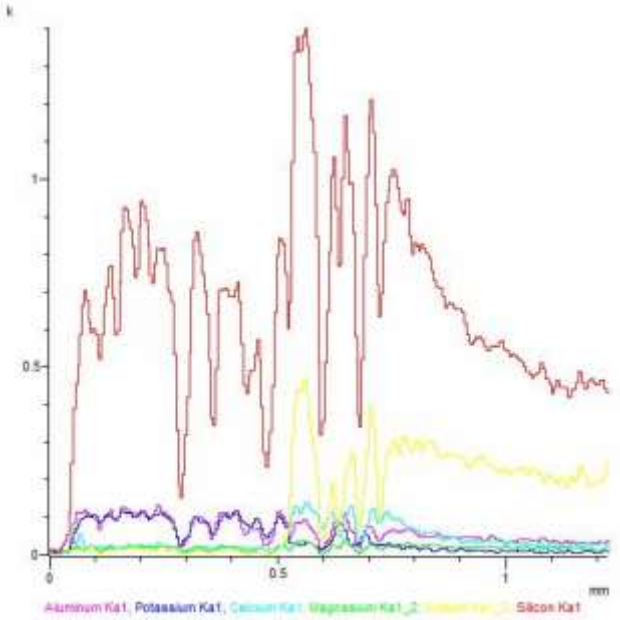

Tesserae 3

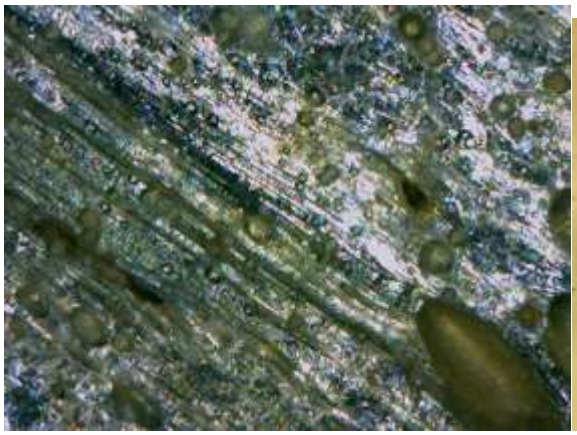

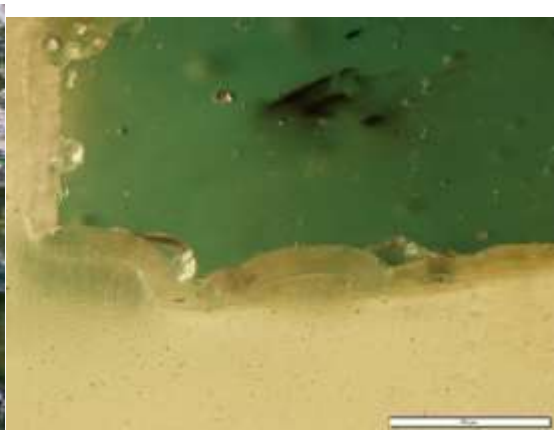

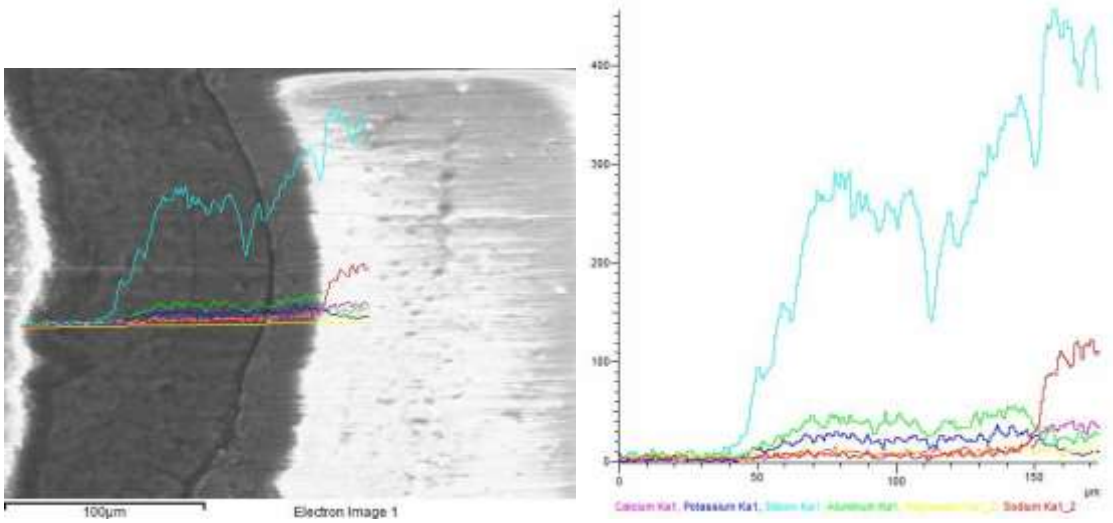

Tesserae 4

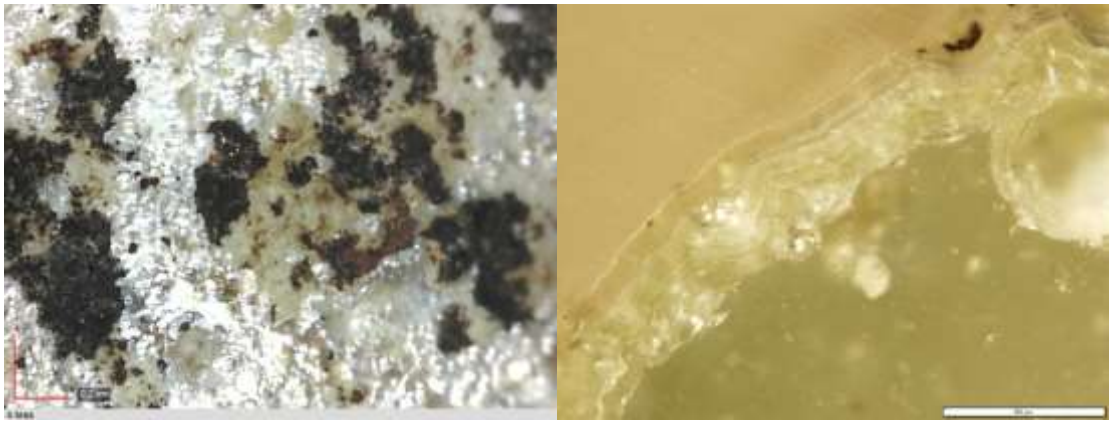

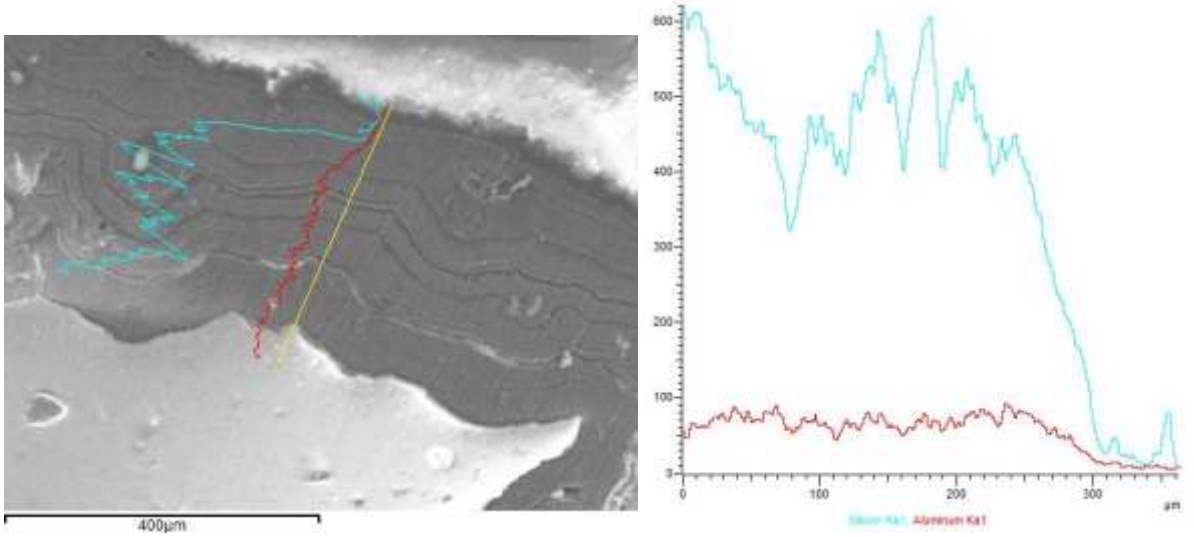

Tesserae 5

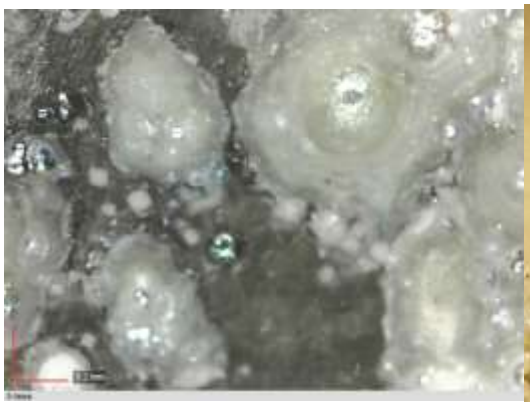

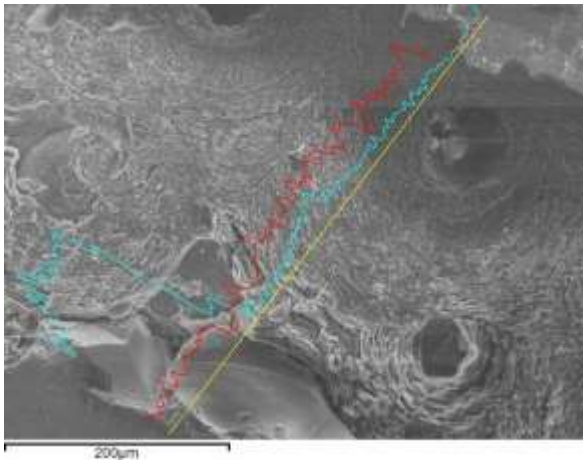

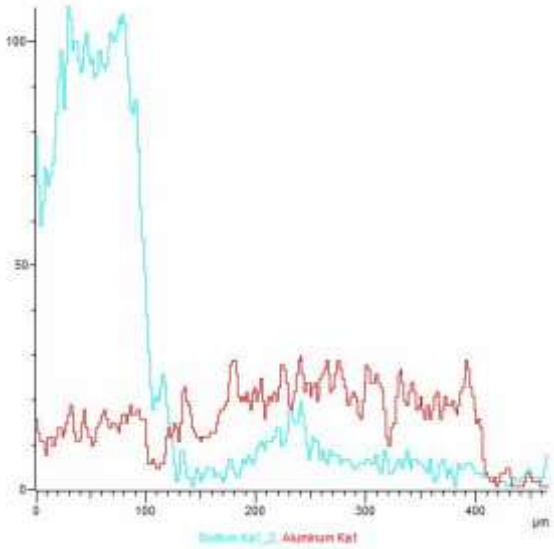

Tesserae 6

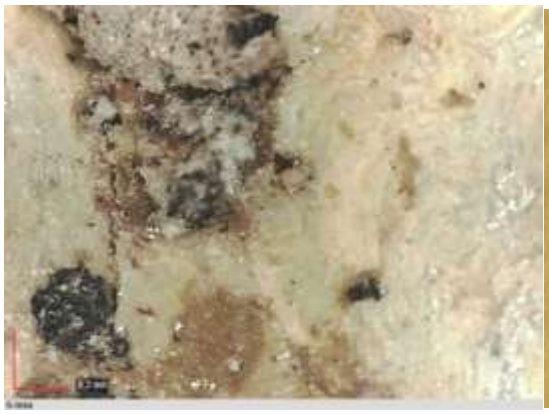

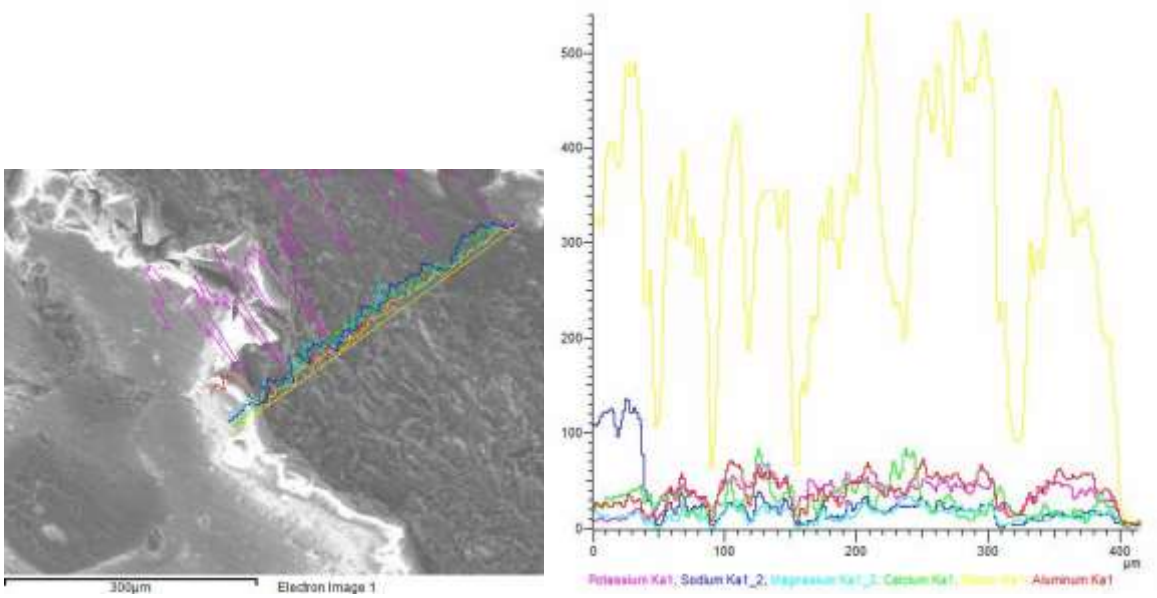

Tesserae 7

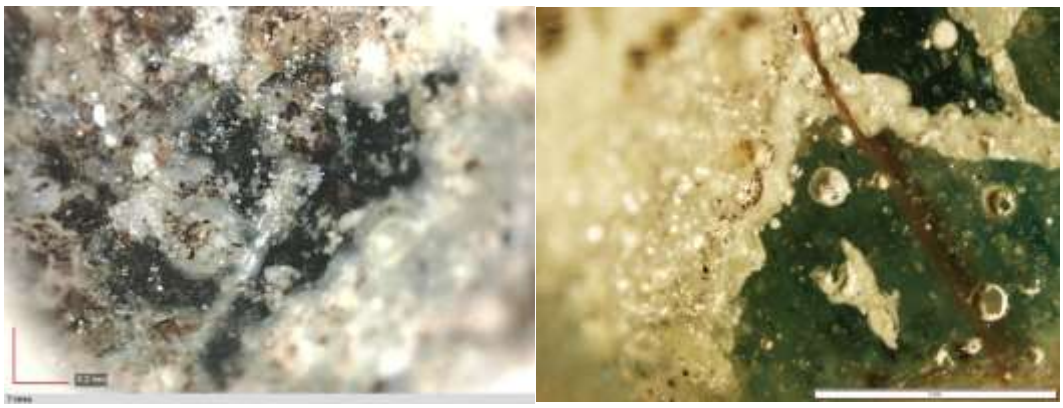

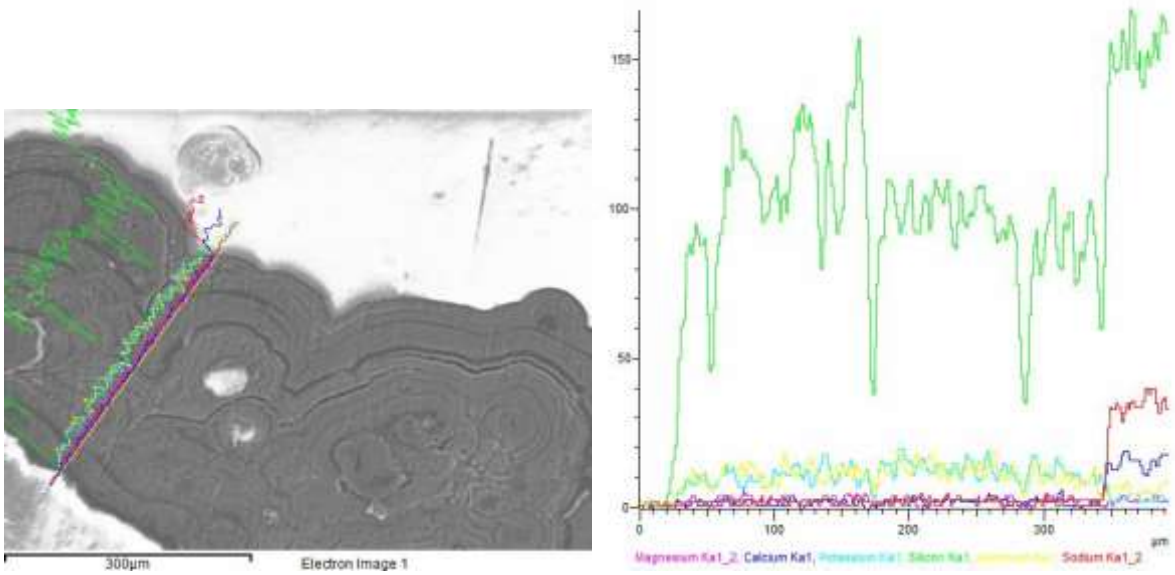

Tesserae 8

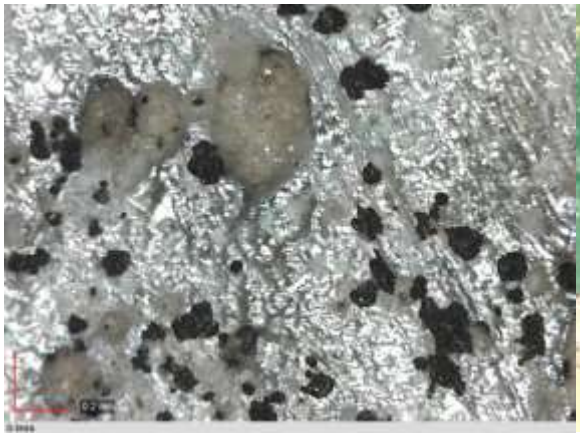

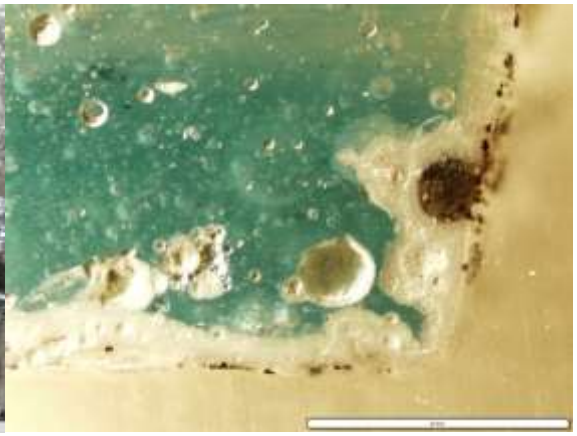

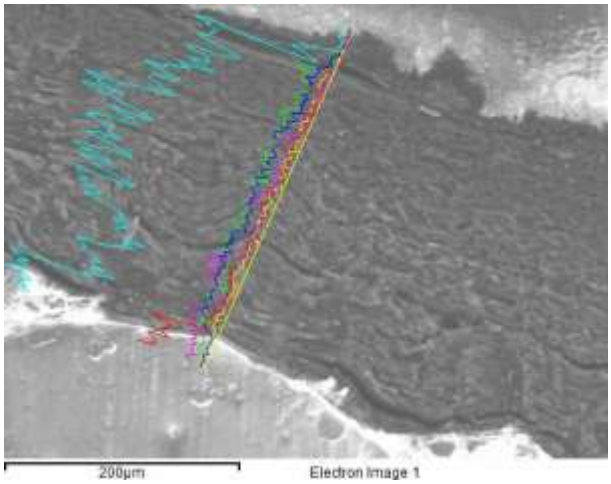
200µm
Electron Image 1

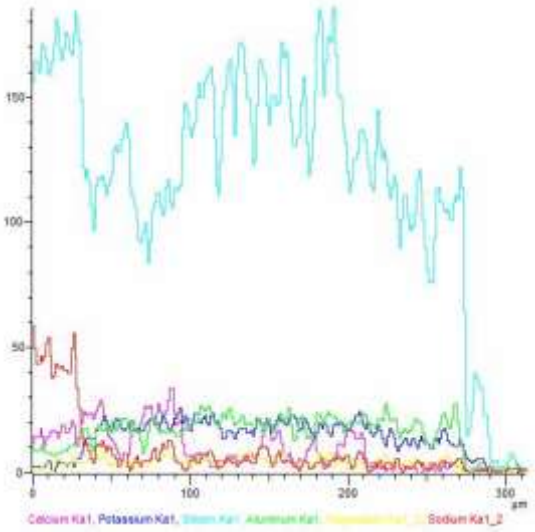
150
100
50
0
0
100
200
300
µm
Calcium Ka1, Potassium Ka1, Sodium Ka1_2

Tesserae 9

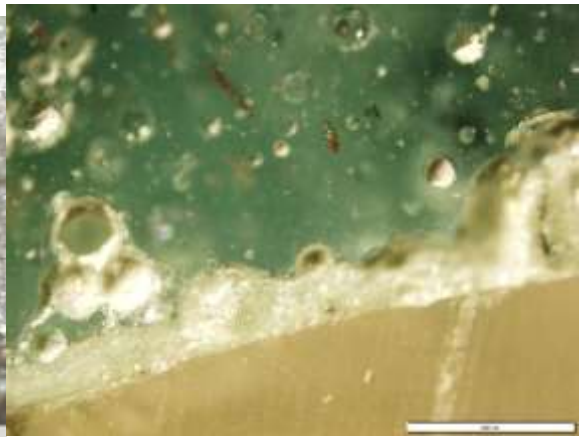

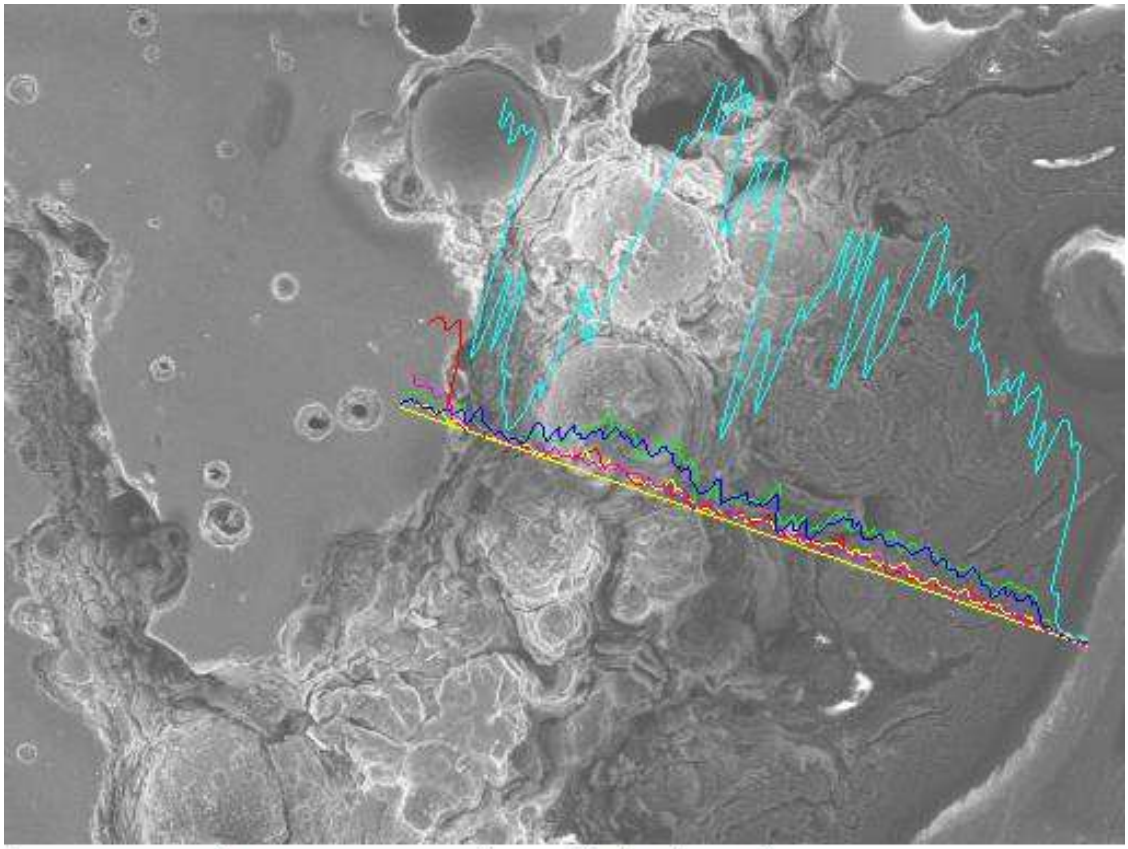

Tesserae 10

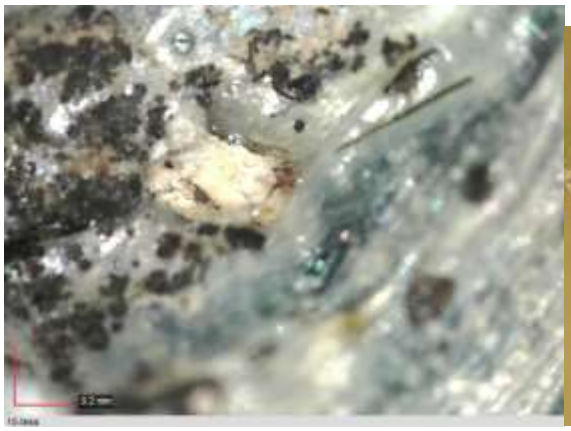

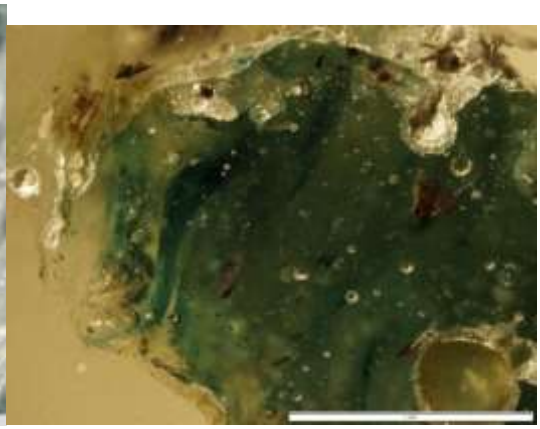

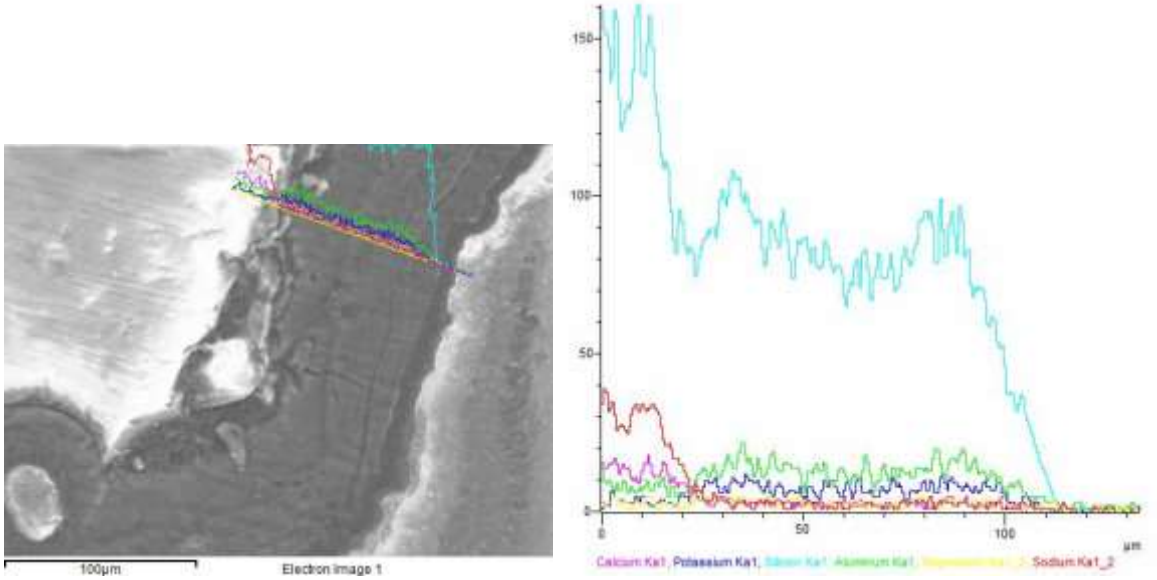

Tesserae 11

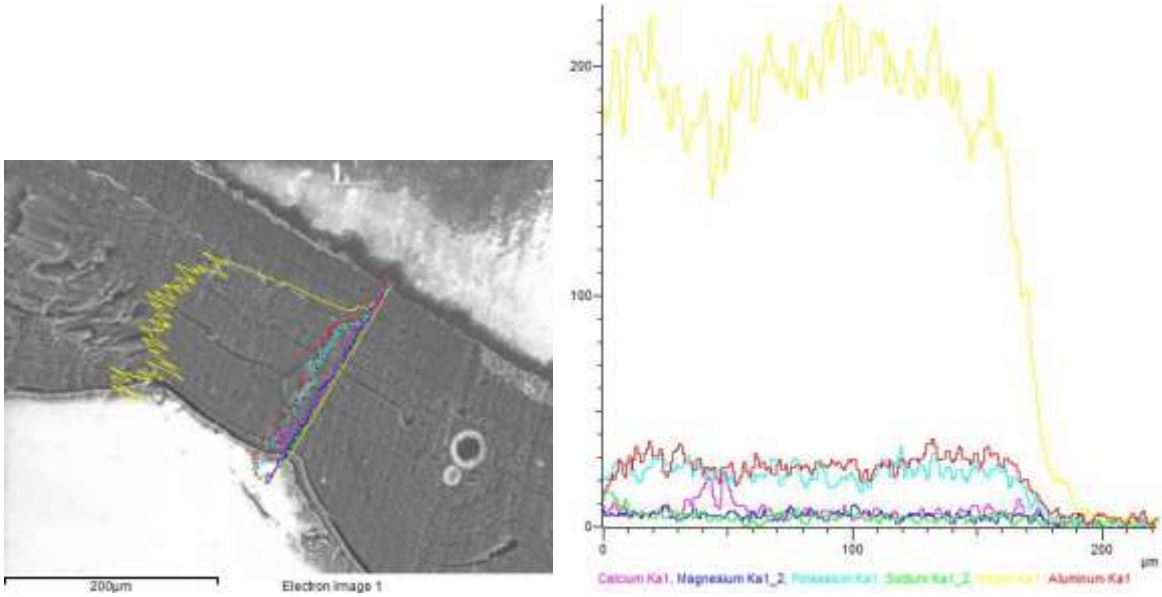

Tesserae 12

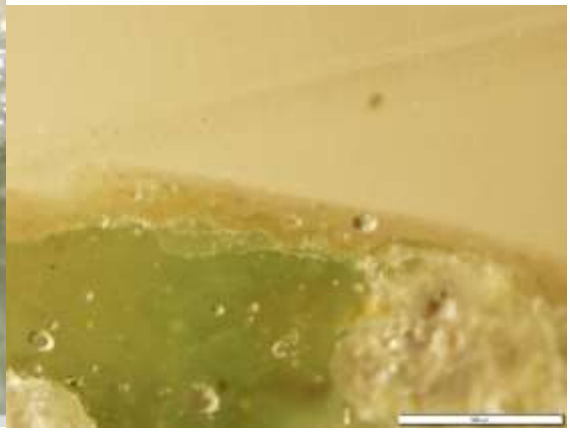

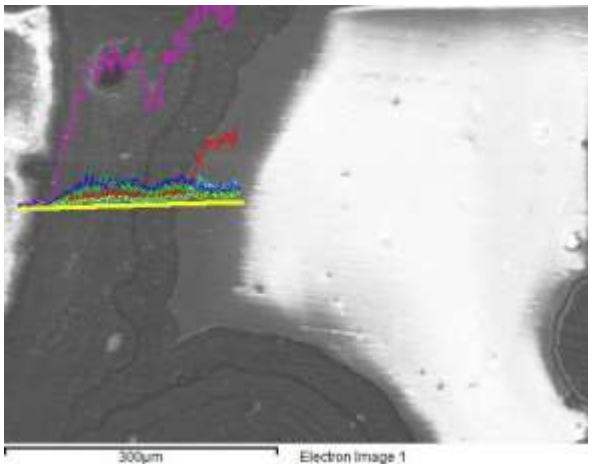

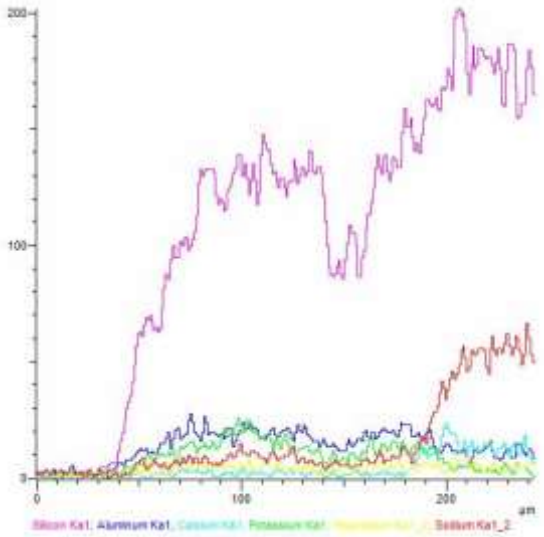

Tesserae 13

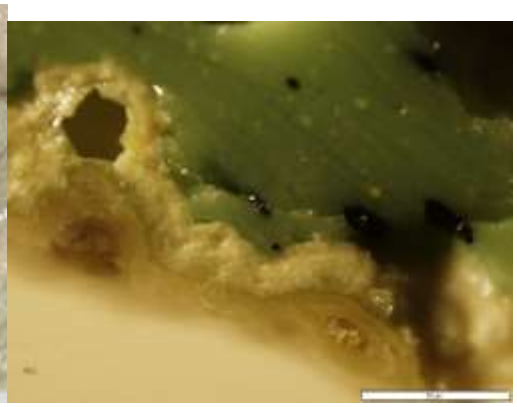

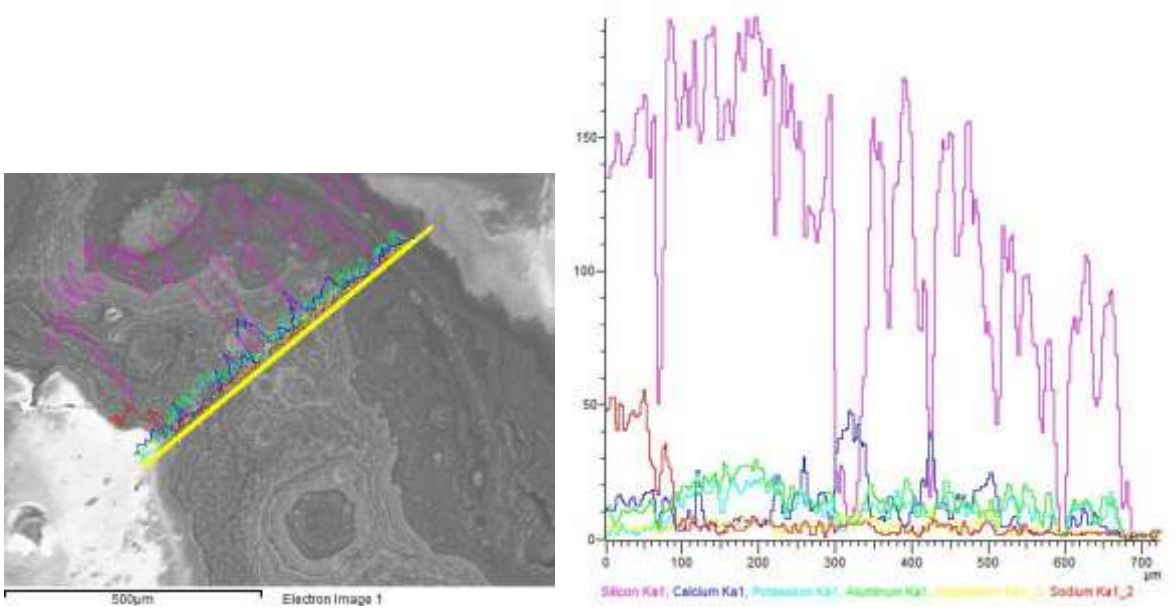
150
100
50
0
0
100
200
300
400
500
600
700
µm
500µm
Electron Image 1
Calcium Ka1
Sodium Ka1_2

Tesserae 14

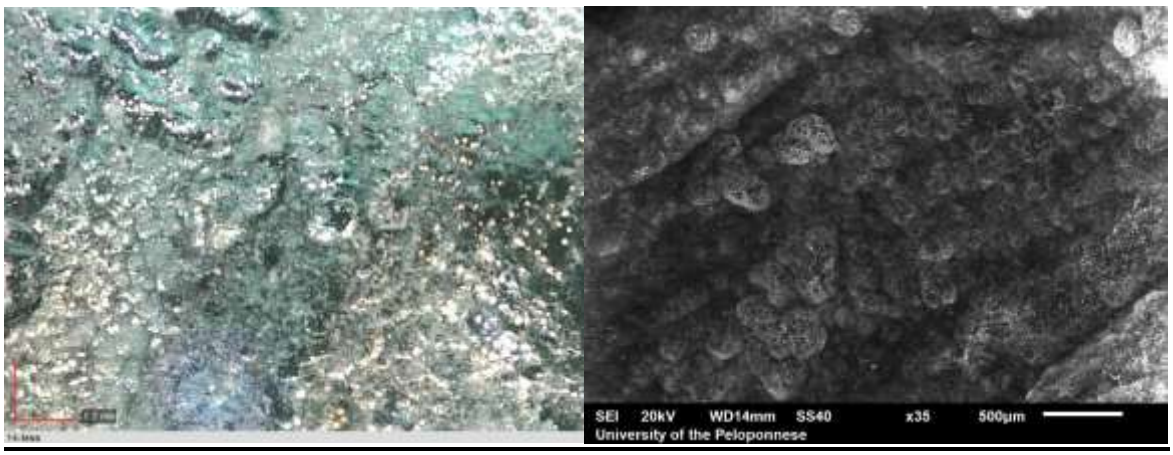
SEI 20kV WD14mm SS40 x35 500µm
University of the Peloponnese

Bibliography

Arletti, R, C. Fiori and M. Vandini. A study of glass tesserae from mosaics in the monasteries of Daphni and Hosios Loukas, Greece. *Archaeometry*. (2010) 52:5. 796-815.

Arletti, R., Simona Quartieri and Giovanna Vezzalini. Glass mosaic tesserae from Pompeii: An Archaeometric investigation. *Periodico di Mineralogica.* (2006) 75,2-3. 25-38.

Arletti, R., Sonia Conte, Mariangela Vandini, Cesare Fiori, et al. Florence baptistery: chemical and mineralogical investigation of glass mosaic tesserae. *Journal of Archaeological Science.* (2011) 38. 79-88.

Artioli, Gilberto. 2010. *Scientific Methods and Cultural Heritage: An introduction to the application of materials science to archaeometry and conservation science*. Oxford: Oxford University Press.

Andronicos, Man. Ancient Greek Painting and Mosaics in Macedonia. Institute for Balkan Studies: University of Thessaloniki. 1964. 287-302.

Barringer, Judith M. Art and Archaeology of Ancient Greece. 2014. Cambridge: Cambridge University Press.

Bellendorf, Paul, Roemich, Hannelore, et al. 2010. *Archaeological glass: the surface and beyond.* Glass and Ceramics Conservation 2010. Interim Meeting of ICOM-CC Working Group. Corning, New York. Accessed January 2010.

Blaszevska, Silvana and Jovan Radnjanski. The Temple of Isis at Stobi. Romanising oriental gods? Religious transformations in the Balkan provinces in the Roman period: New Fins and Novel Perspectives. *Proceedings of the International Symposium, Skopje: 18-21 September 2013*. 215- 257.

Boev, Blazo, Tena Siakova-Ivanova, Mishko Tutkovski and Tome Filov. Mineralogical investigation of the Old Episcopal Basilica in Archaeological Locality of Stobi. Geologica Macedonica: Journal of the Geological Institute at the Faculty of Natural and Technical Sciences, University "Goce Delcev" Stip, North Macedonia. (2016) 30: 1. 33-40. http://eprints.ugd.edu.mk/15932/1/Rektor%20GM%20paper.pdf

Brems, Dieter, Sara Boyen, Monica Ganio et al. Mediterranean Sand Deposits as a Raw Material for Glass Production in Antiquity. *Annales: International Association for the History of Glass.* Thessaloniki. 2009. 120-128.

Caldeira, Bento, Rui Jorge Oliveira, Teresa Teixido, et al. Studying the Construction of Floor Mosaics in the Roman Villa of Pisoes (Portugal) Using Noninvasive Methods: High Resolution 3D GPR and Photogrammetry. *Remote Sensing.* 2019. 11. 1-20. DOI:10.3390/rs11161882

Cholakova, Anastasia, Thilo Rehren. A Late Antique Manganese-Decolourised Glass Composition: interpreting patterns and mechanisms of distribution. Ed. Daniela Rosenow, Matt Phillips, Andrew Meek and Ian Freestone. *Things that Travelled: Mediterranean Glass in the First Millennium CE*. London: UCL Press. 2018. 46-72.

Davison, Sandra. 2003. *The Conservation and Restoration of Glass.* 2nd edition. Oxford: Elsevier Ltd.

Degryse, Patrick et al. Primary Glass Factories around the Mediterranean. *Glass making in the Greco-Roman World: Results of the ARCHGLASS project.* Ed. Patrick Degryse. Leven University Press. 2014. 97-112

Dunbabin, Katherine M.D. Mosaics in the Greek and Roman World. 1999. New York: Cambridge University Press.

Freestone, Ian. Post depositional changes in archaeological ceramics and glasses. *Handbook of archaeological sciences*. Ed. D.R. Brothwell and A.M. pollard. 2001. John Wiley and sons ltd. 615-625.

Folk, Robert, S. Valastro Jr. Radiocarbon Dating of Mortars at Stobi. Ed. James Wiseman and Dorde Mano-Zisi. *Studies in the antiquities of Stobi.* New Jersey: Princeton University Press1983:2. 29-39

Henderson, Julian. Ancient glass: An interdisciplinary exploration. 2013.New York: Cambridge University Press.

International Center for the Study of the Preservation and Restoration of Cultural Property (ICCROM). International Symposium on the Conservation of Mosaics: Deterioration and Conservation. Rome. November 1977.

Jackson, CM, S. Paynter, M.D. Nenna and P. Degryse. Glassmaking using natron from el-Barnugi (Egypt); Pliny and the Roman glass industry. *Archaeol Anthropol Sci.* (2018), 10:11, 1179-1191. DOI: 10.1007/s12520-016-0447-4

Janssens, Koen H. A. 2013 *Modern Methods for Analysing Archaeological and Historical Glass.* United Kingdom: John Wiley & Sons Ltd.

Jackson, CM. Making Colourless Glass in the Roman Period. *Archaeometry.* (2005) 47:4, 763-780.

Kitzinger, Ernst. A Survey of the Early Christian Town of Stobi. *Dumbarton Oak papers*. 1946. 81-162. https://www.jstor.org/stable/1291044

Kolarik, Ruth. Mosaics of the Early Church at Stobi. *Dumbarton Oaks Papers.*41: 1987. 295-306. http://www.jstor.org/stable/1291567

Kolarik, Ruth. The Floor Mosaics of Eastern Illyricum. Εισηγησεις του Δεκατου Διεθνους Συνεδριου Χριστιανικης Αρχαιολογιας (Thessaloniki 28 September -4 October 1980) 173-203.

Kolarik, Ruth, and Momcilo Petrovski. Technical Observations on Mosaics at Stobi. *Studies in the Antiquities of Stobi.* Ed James wiseman and Dorde Mano-Zisi.New Jersey: Princeton University Press, 2: 1983.

Lee, C. and D.E. Clark. Characterization of Glass Surfaces. *Applications of Surface Science*. 1984. 397-412.

Livy Ad Urbe Condita
http://www.perseus.tufts.edu/hopper/text?doc=Perseus:abo:phi,0914,00133:19:18

Janssens, Koen. Modern Methods for Analysing Archaeological and Historical Glass. United Kingdom: John Wiley and Sons Ltd. 2013.

Palamara, Eleni, N. Zacharias, L. Papakosta, D. Palles, E.I. Kamitsos & J. Pérez-Arantegui. Studying a Funerary Roman Vessel Glass Collection from Patras, Greece: An Interdisciplinary Characterisation and Use Study, *STAR: Science & Technology of Archaeological Research,* (2016) 2:2, 203-216. DOI: 10.1080/20548923.2016.1239868

Pliny. *Natural History, Volume X: Books 36-37.* Translated by D. E. Eichholz. Loeb Classical Library 419. Cambridge, MA: Harvard University Press, 1962. https://www.loebclassics.com/view/LCL419/1962/volume.xml

Pollard, A.M., Heron, Carl. 1996. *Chapter 5: Chemistry and Corrosion of Archaeological Glass.* Archaeological Chemistry. Cambridge: Royal Society of Chemistry.

Radnjanski, Jovan. Archaeologist at Stobi. Dimitar Nikolovski, typologist of Glass at Stobi. Personal communication. E-mail. 2019.

Rasmussen, Seth C. How Glass Changed the World: The History of and Chemistry of Glass from Antiquity to the 13th Century. Springer Briefs in Molecular Science. New York: Springer. 2012.

Robertson, Martin. Greek Mosaics. *Journal of Hellenic Studies.* (1965) 85. 72-89. https://www.jstor.org/stable/628810

Freestone, Ian et al. HIMT, Glass Composition and commodity branding in the primary glass Industry. Ed. Daniela Rosenow, Matt Phillips, Andrew Meek and Ian Freestone. *Things that Travelled: Mediterranean Glass in the First Millennium CE*. London: UCL Press. 2018. 159-191.

Scott, R.B., Patrick Degryse. The archaeology and archaeometry of natron glass making. *Glass making in the Greco-Roman World: Results of the ARCHGLASS project.* Ed. Patrick Degryse. Leven University Press. 2014. 15-26

Sokolovska, Viktorija. Investigations in the House of Peristerias. *Studies in the Antiquities of Stobi Volume 2.* Ed James Wiseman and Dorde Mano-Zisi. Beograd: 1975.

Smith, Ray Winfield. The Significance of Roman Glass. *The Metropolitan Museum of Art Bulletin.* 49-60.

Tait, Hugh. Five Thousand Years of Glass. London: The British Museum Press. 2012.

Tutkovski, Misko. Paintings in the Old Episcopal Basilica in Stobi: Analyses of the Technical-Technological Characteristics. *Folia Archaeologica Balkanica: Institute of Art History and Archeology, Skopje*. 4: 2018. 377- 403.

Map of stobi https://mymacedoniablog.wordpress.com/sightseeing/archeological-sites/stobi/

Muros, Vanessa, et al. *Objects Speciality Group Conservation Wiki: Glass.* American Institute for Conservation Wiki. Accessed January 2019. http://www.conservation-wiki.com/wiki/Glass#Deterioration

Vataj, Esmerelda, Elio Hobdari, et al. Analytical characterization of glass tesserae from mosaics of Early Christian basilicas in Albania. *Applied Physics A.* (2017) 123:76. 1-15. DOI: 10.1007/s00339-016-0661-z

Verri, Giovanni, Paul Roberts, et al. Investigating the Construction Methods of an Opus Vermiculatum Mosaic Pane. *British Museum: Technical Research Bulletin.*2010: 4. 1-13.

Wiseman, James. Archaeology and History at Stobi, Macedonia. *Rome and the Provinces: Studies in the Transformation of Art and Architecture in the Mediterranean World.* Ed Charles B. McClendon. New Haven Society of the Archaeological Institute of America. 1986. 37-50.

Wiseman, James and Djordje Mano-Zisi.Stobi: A City of Ancient Macedonia.*Journal of Field Archaeology.* (1976) 3:3, 269-302. http://www.jstor.org/stable/529437

Wiseman, James. Stobi in Yugoslavian Macedonia: Archaeological Excavations and Research, 1977-78. *Journal of Field Archeology*. (1978) 5:4, 391-249. http://www.jstor.org/stable/529493

Worthington, Ian, and Joseph Roisman. A Companion to Ancient Macedonia. 2013. Oxford: Blackwell publishing Ltd.

Zeitzer, Ryan. The Roman Glass Industry: An Analysis of Roman Era Glass Production and the Lives of Glassblowers. 2018. *Master's Thesis*. Brandeis University.